UC Irvine

UC Irvine Electronic Theses and Dissertations

Title

Plasma Wakefield Acceleration of Ultra-High Energy Particles in Astrophysical Jets

Permalink

https://escholarship.org/uc/item/5cd1t04s

ISBN

9798173723031

Author

Huxtable, Gregory Barton

Publication Date

2024-11-03

Peer reviewed|Thesis/dissertation

eScholarship.org Powered by the California Digital Library
University of California

UNIVERSITY OF CALIFORNIA,
IRVINE

Plasma Wakefield Acceleration of Ultra-High Energy Particles in Astrophysical Jets

DISSERTATION

submitted in partial satisfaction of the requirements
for the degree of

DOCTOR OF PHILOSOPHY

in Physics

by

Gregory Barton Huxtable

Dissertation Committee:
Professor Zhihong Lin, Chair
Professor Toshiki Tajima
Professor Peter Taborek

2024

© 2024 Gregory Barton Huxtable

TABLE OF CONTENTS

Page

LIST OF FIGURES iii

LIST OF TABLES v

ACKNOWLEDGMENTS vi

VITA vii

ABSTRACT OF THE DISSERTATION ix

1 Introduction 1
- 1.1 Astrophysical Jets . . . 1
- 1.2 UHE Emissions . . . 3
- 1.3 Wakefield Acceleration . . . 6
- 1.4 Accretion disk Dynamics . . . 9

2 Wakefield Acceleration in Jets 16

3 Test Cases 26
- 3.1 Blazar: TXS 0506+056 . . . 26
- 3.2 Radio Galaxy: Centaurus as A . . . 30
- 3.3 Seyfert Galaxy: NGC 1068 . . . 31
- 3.4 Starburst Galaxy: M82 . . . 34
- 3.5 Starburst Galaxy: NGC 0253 . . . 36
- 3.6 Microquasar: SS 433 . . . 38

4 Conclusions 40
- 4.1 Applications . . . 40
- 4.2 Wakefield Acceleration in AGN Jets . . . 42

Bibliography 48

Appendix A Model Dependence on Arbitrary Jet Spreading Index 59

LIST OF FIGURES

Page

1.1 Over the timescale of the disc's orbital period, the axial magnetic field will develop twisted, concentric layers of helical fields, where the inner layers having a greater wrapping pitch than outer layers due to the differential rotation of the accretion disk (from [135]). 4

1.2 VLA image of the radio galaxy Cygnus A (3C 405) with its jets and giant radio lobes (credit: NRAO/AUI). Matter is accreted from the inner disk (central bright dot) orbiting the central black hole and subsequently expelled, creating bipolar jets (right and left thin lines extending from the accretion disk). It is visually evident that the jets are stable (absence of plasma instabilities) for the majority of their length, until their kinetic energy has depleted substantially and begins to interact with the ambient plasma, forming turbulent gaseous lobes (top right and lower left cocoon) at the end of both jets. We consider wakefield acceleration in the thin, elongated jet. 4

1.3 Classic 1D PIC simulation of wakefield depicting the trailing electrostatic field in red, electron density in blue, and the driving laser pulse in yellow. The clear coherency due to the high phase velocity (in fact relativistic) wakefields is demonstrated (from [136]). 7

1.4 The physical consequences of the magneto-rotational instability. A) Magnetic field is amplified by the winding motion due to the differential rotation of the accretion disk. When the field strength becomes too resistive for the accretion disk to maintain steady-state Keplerian rotation, a sudden, massive accretion event occurs, causing the field to snap back to the less magnetized state, emitting an Alfvénic burst as a result (from [55]). B) Magneto-Rotational Instability (MRI) produces an electro-static field, which accelerates charged particles and heats up the disk halo. They eventually produce low energy photons in keV-MeV energy range (from [63]). 11

2.1 WFA theory for the accreting black hole-jet system of an AGN (from [67]). A) The cross section of an AGN, its accretion disk and jets. Alfvén waves generated upon large mass accretions at the base of the jet propagate along the field line of the jet. They eventually mode-convert into intense electromagnetic waves when the wave frequency matches the local plasma frequency, $\omega'_{\rm p} = (4\pi n_{\rm jet} e^2/m_{\rm e}\gamma\Gamma^3)^{1/2}$, where γ is the Lorentz factor of a trapped particle, and Γ is the bulk Lorentz factor of the jet. B) The structure of the bow wake. An electron cloud is formed at the front (top) of the wave pulse and a proton cloud follows. The resultant electric field accelerates protons in the back side and electrons in the front side of the bow wake. Since this acceleration structure moves at a velocity close to the speed of light, the charged particles with the same velocity (light velocity) in the field are accelerated for a long time and distance. 17

2.2 Plot of frequencies versus distance from the accretion disk normalized by the radius of the innermost stable circular orbit, where log here is base 10 (from [46]). The frequency of the emitted Alfvén wave $\omega_{\rm A}$, relativistic plasma frequency $\omega'_{\rm p}$, and relativistic electron cyclotron frequency $\omega'_{\rm c}$ are shown. When the (orginally of Alfvénic type) wave reaches the overdense plasma $\omega_A > \omega'_p$ it mode converts to a more typical electromagnetic wave, and wakefield acceleration occurs, if not before then. 19

2.3 The maximum energies of protons, $W_{\rm max}$, are predicted using the mass of the central black hole (normalized by one solar mass), m, on the right abscissa, and total radiation luminosity, $L_{\rm rad}$, by the wakefield acceleration theory [136] on the left abscissa. Various astronomical objects, such as microquasars ($m = 1 \sim 10$), ultra luminous X-ray sources (ULXs; $m = 100 \sim 10000$) in starburst galaxies, central blackholes of Seyfert galaxies $m \sim 10^6$ and radio galaxies/blazars ($m = 10^7 \sim 10^{10}$) can accelerate UHECRs with energy above 10^{20} eV. The individual points (or boxes) are plotted based on their known (or estimated) central mass according to our theory. Here, we assume the charge is $z = 1$, the bulk Lorentz factor of the flow of the jets $\Gamma = 10$, and $\alpha = 0.1$ the "α" parameter of the disk. From top to bottom, the three dashed lines represent $\dot{m} = 10^{-1}$, 10^{-3}, and 10^{-5} (from [67]). 20

3.1 Prominent candidates of pin-pointed UHECR emission (from [67]). Based on morphology of the candidates and their existing data, WFA theory predicts M82, NGC0253, Cen A, and NGC4945 are promising UHECR sources. The three hot spots in the observed skymap (red circles) of UHECRs $> 6 \times 10^{19}$ eV [1] are consistent with prediction. 32

4.1 Upon the merger of two colliding neutron stars, gravitational waves are emitted, followed by a long-duration gamma-ray burst. Takahashi predicted that this dense burst of gamma-rays creates an extremely intesne bow-wake capable of creating a substantial flux of extremely high-energy cosmic-rays with energies exceeding 10^{21} eV. (from [137]). 43

LIST OF TABLES

Page

2.1 Time Scales, Maximum Energy, and Luminosities estimates (see Huxtable *et al.* [67]) 22

3.1 Comparison of observed parameters (shaded) and theoretical parameters (without shade). Taken from Huxtable *et al.* (2023) [67]. Theoretical and observational values for a range of astrophysical objects, including a blazar (BL), a radio galaxy (RG), a Seyfert galaxy (SyG), starburst galaxies (SBG) and a micro-quasar (MQ). 30

ACKNOWLEDGMENTS

I would like to thank my advisor, Professor Toshiki Tajima, for his supervision of my Ph.D and for his persistent encouragement. I would also like to thank my elder academic brother, Scott Nicks, for his mentorship these past six years, particularly during my internships with TAE Technologies, and for always taking time out of his day to offer advice, or empathy when I needed it. And to my academic brothers Ernesto Barraza-Valdez and Gabe Player, for their camaraderie throughout our time together at UCI.

I am grateful to my father, Barton D Huxtable, for inspiring in me a genuine appreciation for the laws of the natural world, and for instilling in me a confidence, free of hubris, that I have fallen back on time and again when faced with adversity. As well as my mother, Jacqueline Huxtable, for her unconditional love and support throughout my life. And finally, Miranda Weissman, who has been my rock these past several years, thank you from the bottom of my heart.

This work was done at the University of California, Irvine, with the supports of the Norman Rostoker Chair Fund (Toshiki Tajima) and TAE Technologies subcontract.

Portions of this dissertation is a reprint of the material as it appears in "G. B. Huxtable, N. Eltawil, W. X. Feng, G. Player, W. Wang, T. Tajima and T. Ebisuzaki, Signatures of Wakefield Acceleration in Astrophysical Jets via Gamma-Rays and UHECRs, MNRAS, (2023)", © 2023 Oxford University Press, https://doi.org/10.1093/mnras/stad1303, used with permission of Oxford University Press.

VITA

Gregory Barton Huxtable

EDUCATION

Doctor of Philosophy in Physics — **2024**
University of California, Irvine — *Irvine, California*

Bachelor of Science in Physics and Mathematics — **2018**
University of Maryland, Baltimore County — *Baltimore, Maryland*

RESEARCH EXPERIENCE

Graduate Research Assistant — **2020–2024**
University of California, Irvine — *Irvine, California*

Undergraduate Research Assistant — **2016–2018**
University of Maryland, Baltimore County — *Baltimore, Maryland*

NASA Student Research Assistant — **2016**
NASA Goddard Space Flight Center — *Greenbelt, Maryland*

TEACHING EXPERIENCE

Teaching Assistant — **2018–2019**
University of California, Irvine — *Irvine, California*

REFEREED JOURNAL PUBLICATIONS

Signatures of wakefield acceleration in astrophysical jets via gamma-rays and UHECRs **2023**
Monthly Notices of the Royal Astronomical Society

G. B. Huxtable, N. Eltawil, W. X. Feng, G. Player, W. Wang, T. Tajima and T. Ebisuzaki

High-Density Dynamics of Laser Wakefield Acceleration from Gas Plasmas to Nanotubes **2021**
Photonics

B. S. Nicks, E. Barraza-Valdez, S. Hakimi, K. Chestnut, G. DeGrandchamp, K. Gage, D. Housley, G. Huxtable, G. Lawler, D. Lin, P. Manwani, E. Nelson, G. Player, M. Seggebruch, J. Sweeney, J. Tanner, K. Thompson and T. Tajima

A Study of the 20 day Superorbital Modulation in the High-mass X-Ray Binary IGR J16493-4348 **2019**
The Astrophysical Journal

J. B. Coley, R. H. D. Corbet, F. Fürst, G. Huxtable, H. A. Krimm, A. B. Pearlman and K. Pottschmidt

ABSTRACT OF THE DISSERTATION

Plasma Wakefield Acceleration of Ultra-High Energy Particles in Astrophysical Jets

By

Gregory Barton Huxtable

Doctor of Philosophy in Physics

University of California, Irvine, 2024

Professor Zhihong Lin, Chair

Ultra-high energy cosmic rays (UHECRs) are the most energetic particles known to exist, reaching energies as high as 10^{20} eV – a firm cutoff due to the GZK limit. It is believed that many of these particles originate in the jets of active galactic nuclei (AGN). Plasma wakefields propagating along AGN jets, driven by extremely intense electromagnetic pulses (whose Lorentz invariant vector potential may range from $10^6 - 10^{10}$) are argued to be a likely mechanism capable of generating ultra-high energy (UHE) charged particles, in addition to UHE neutrinos and gamma-rays as a result of collisions, among other emission types. A wakefield acceleration (WFA) model is developed in an effort to shed light on the origin of the these signals. It is posited that wakefield acceleration in conjunction with the magneto-rotational instability of the accretion disk explains both structural properties of the jets and details in their emission signals, such as correlations in neutrino and gamma-ray bursts, and in the case of blazars, anti-correlations in flux and spectral index. Furthermore, the model presented herein predicts an upper bound for the energy of UHECRs emitted from a source given the mass of its central compact object and total jet luminosity. Six case studies from a comprehensive mass range ($1 - 10^9\ M_\odot$) of astrophysical objects, each of which possess jets, emit high-energy gamma radiation and in some instances spatially identifiable UHECRs. All sources are strong candidates for UHECR emission, if not already known to emit them. To provide context for our model predictions we quantitatively compare them

with observational data. Since the accretion and acceleration mechanisms are independent of mass, aside from determining maximum values, blazars ($\sim 10^9\ M_\odot$), radio galaxies ($\sim 10^8\, M_\odot$), Seyfert galaxies ($\sim 10^6\, M_\odot$), starburst galaxies ($\sim 10^3\, M_\odot$), even microquasars ($1 \sim 10\ M_\odot$) interestingly exhibit the same physics.

Chapter 1

Introduction

1.1 Astrophysical Jets

The effect of magnetic fields cannot be ignored when trying to understand the dynamics of astrophysical plasmas in relatively small (e.g. solar dynamo) or large (e.g. galactic disc-jet structures) scales as Hannes Alfvén himself pointed out, see, for example, his book *Cosmic Plasma* [20], specifically Figs. II.9 and II.10. Subsequent research has demonstrated their importance in the generation of massive cosmic structures. Lovelace and Blandford [86, 30], and Uchida and Shibata [142, 127, 128] showed that the presence of an axial magnetic field in an accretion disk can generate extremely long jets, in many cases longer than the host galaxy (or binary star) is wide. Galaxies that host jets are colloquially known as active galactic nuclei (AGN) of which perhaps a surprisingly large number of galaxies are categorized. The shear size of AGN jets, and the fact that they are well-contained and stable against otherwise destructive instabilities suggests that an extremely energetic force is present. In this dissertation it is posited that jets and their ultra-highly energy (UHE) emissions cannot be understood as an independent system on a local scale, but instead a single, global system

in synchronicity with the host accretion disk from which the jets are created.

A great deal of research has been done in an effort to decipher the nature cosmic plasmas. For example, Kennel *et al.* developed numerical magnetohydrodynamics (MHD) simulations of cosmic plasmas [83, 84] that illustrated magnetic fields essential role in determining global topology of magnetospheres, while also pointing out their influence on small-scale astrophysical plasmas. Alfvén pointed out the filamentary nature of cosmic plasma, Uchida and Shibata demonstrated how AGN jets are born out of accretion discs, and Leboeuf *et al.* observed a shock cone, among many other works. In this dissertation, Uchida and Shibata's work on jet formation from an accretion disk (a global MHD model) lies at the heart of the subsequent model for estimating UHE emissions of jets. It is possible that kinetic effects could give rise to the dynamo effects that spontaneously produce magnetic fields out of non-magnetized plasma (see e.g. Ref. [99]). However, barring such microscopic effects, it is worth pointing out that nonmagnetic, gravitational dynamics of accretion discs cannot produce jets. This should hopefully convince the reader that the role magnetic fields play in disc-jets systems is of great significance.

When there is a static constant axial magnetic field, B_z, originally penetrating the accretion disk plasma, the rotational motion of the accretion disk twists the magnetic field, which creates an azimuthal component of the field, B_θ (e.g. Fig. 4.17 in [135]). These axially oriented fields may be from already present intergalactic fields, or from plasma turbulence within the disk itself. Distortion of the originally uniform B_z field gives rise to the radial inward current J_r through Ampere's law,

$$\frac{4\pi}{c}\boldsymbol{J} = \nabla \times \boldsymbol{B}. \tag{1.1}$$

The Lorentz force due to the radial current and azimuthal magnetic field then accelerates plasma in the axial direction ($\hat{z}$), perpendicular to the accretion disc,

$$\boldsymbol{f} = \frac{1}{c}(\boldsymbol{J} \times \boldsymbol{B}). \tag{1.2}$$

This force is what generates a steady stream of plasma emanating out of the disc. The longitudinal magnetic field, B_z, and the induced toroidal field, B_θ, generate the helical field structure of the jets as plasma is forced in the axial directions. Furthermore, the wrapping pitch increases near the center of the disk due to differential (Keplerian) rotation, giving rise to a remarkably well-collimated structure we know as "jets." See, for example, works by Shibata *et al.* and Matsumoto *et al.* [128, 128, 92], and Fig. 1.1. These jets can extend as far as nearly a Mpc in length, as in the case of Cygnus A (see Fig. 1.2), in many instances much longer than the width of their host galaxies' accretion disc. The interplay between the immense gravitational pull of the central accreting engine, a super-massive black hole (SMBH) (or a neutron star, NS, in the case of some microquasars), it's rotating accretion disc, and intricately woven jets, which guide plasma away from the center along the axes, maintains the stable disc-jet structure. Eventually the speed of plasma must slow down due to inherent collisions with interstellar gases and in turn form large lobes, or plumes at the end of the jets, where turbulent beam-plasma instabilities dominate the otherwise coherent stream of plasma.

1.2 UHE Emissions

Ultra-high energy cosmic rays (UHECRs) are the most energetic particles known to exist, reaching energies as high as 10^{20} eV – a firm cutoff due to the GZK limit. It is believed

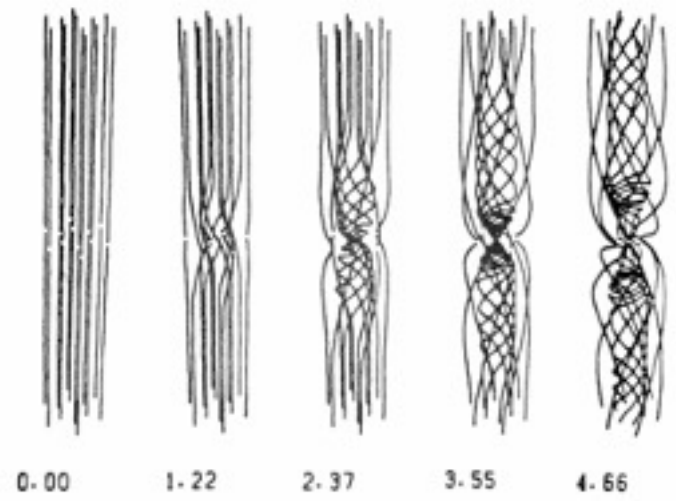


Figure 1.1: Over the timescale of the disc's orbital period, the axial magnetic field will develop twisted, concentric layers of helical fields, where the inner layers having a greater wrapping pitch than outer layers due to the differential rotation of the accretion disk (from [135]).

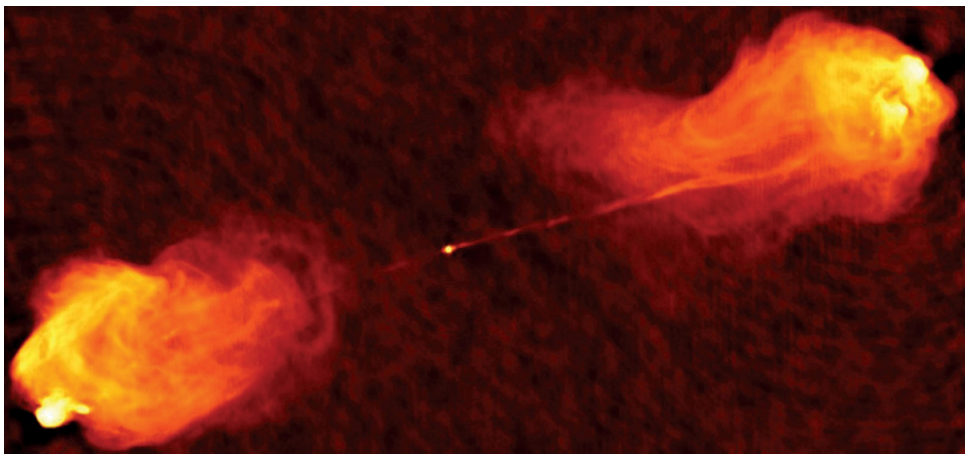


Figure 1.2: VLA image of the radio galaxy Cygnus A (3C 405) with its jets and giant radio lobes (credit: NRAO/AUI). Matter is accreted from the inner disk (central bright dot) orbiting the central black hole and subsequently expelled, creating bipolar jets (right and left thin lines extending from the accretion disk). It is visually evident that the jets are stable (absence of plasma instabilities) for the majority of their length, until their kinetic energy has depleted substantially and begins to interact with the ambient plasma, forming turbulent gaseous lobes (top right and lower left cocoon) at the end of both jets. We consider wakefield acceleration in the thin, elongated jet.

that many of these particles originate in the jets of active galactic nuclei (AGN). Some of these UHE particles may travel to Earth's atmosphere and upon doing so become UHECRs, creating a cascade of subatomic particles and photons, detectable by ground-based observatories, when they collide with atmospheric particles. A wide scope of astrophysical objects ranging from blazars, radio galaxies, Seyfert galaxies, starburst galaxies, and even microquasars emit intense high energy gamma rays ($\geq$ 10 GeV), often in spatially (localized) and temporally identifiable fashions. From each respectable class we chose to study at least one object that is known to host jets – columns of accelerated plasma extending from the poles of the central compact object (either a black hole or neutron star) – as case studies to quantitatively compare their emissions with our theory. Wakefield acceleration (WFA) primarily has implications on UHECRs, UHE neutrinos and gamma-rays, and X-rays, but the theory has milder implications on optical-band light and radio emissions. Most of the selected objects emissions are spatially localized. Some also exhibit temporal structure in their signals, characteristic of WFA. The emissions often are created simultaneously, such as the coincidental "bursts" of high energy gamma rays and neutrinos recently detected in blazar TXS 0506+056 [68, 54, 121].

The high energy phenomena associated with accreting blackholes has been observed with gamma-ray emission. First, The Fermi Gamma-ray Space Telescope, formerly GLAST (Gamma-ray Large Area Space Telescope) launched in 2008 [96] observed accreting blackholes such as active galactic nuclei (AGN) and binary blackholes in the GeV-100 GeV region [7, 14, 15]. In addition, air Cherenkov telescopes, such as MAGIC [45], H.E.S.S. [45], or VERITAS [116] and water Cherenkov detector such as High Altitude Water Cherenkov (HAWC) observatory [43] observed accreting blackholes in TeV and multi TeV gamma rays.

Cosmic rays vary from modest to extremely high energies ($5 * 10^{19}$ eV and beyond). The conventional theory of first-order Fermi shock acceleration has been successful in explaining the universal spectral index of approximately 2 [78] for UHECR energy. However, beyond

10^{19} eV, protons begin to radiate their energies in very large quantities due to synchrotron radiation if they are bent by magnetic fields (as required by Fermi acceleration) or other collisions, since the radiated energy scales quarticly with the Lorentz factor of the particle [71]. Nonetheless, observations have detected UHECRs with energies beyond 10^{20} eV coming from localized origins [11, 64, 44]. Wakefield accelerates particles collinear to the propagation of the wave (see figure 1.3) and therefore they suffer no inherent energy loss. This also implies UHE signals generated by WFA should be emitted axially from the jets.

1.3 Wakefield Acceleration

Ebisuzaki and Tajima suggested that an massive accretion event (following the eruption of the disk due to an instability), at the root of the jet formation region would give rise to a strong excitation of the otherwise steady emanation of the jet flow, which leads to the formation of the large collective plasma wave excitations as a result of an extremely intense electromagnetic (EM) pulse and their further collective behavior in the jet plasma (see Fig 2.1) [46, 47]. As the jet flows accompany the woven fabric of the helical magnetic fields, should disk eruptions occur episodically, so to would excitations of Alfvén waves (or shocks) beginning at the root of the jets, which would then propagate outward along the jet. These Alfvén shocks also give rise to a new structure formation, called wakefields, that trail behind in the *wake* of the driving wave. The Alfvén waves (or shocks) group, and phase velocities are often very close to the speed of light due to the low plasma density and strong magnetic field within the jet. Even if it is not, we will consider that these Alfvén waves tend to eventually mode convert into an extremely intense electromagnetic pulse (as the density and the magnetic field that sustain the Alfvén wave decrease along the length of the jet). We will see the implications of this as a spectacularly self-organized motion and structure formation that is due largely to the highly relativistic motion of the wave and it's extreme intensity.

We find that such relativistic entities tend to show robust structural and dynamical stability and resilience [133]. This is why the wave can in theory propagate to the end of its jets.

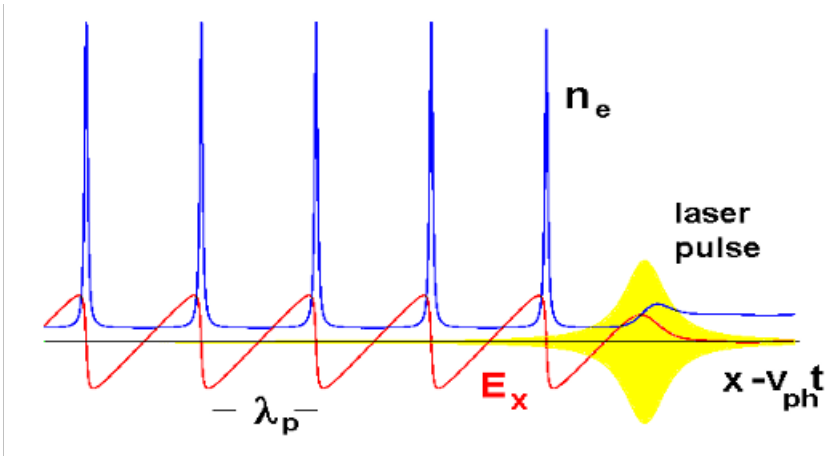


Figure 1.3: Classic 1D PIC simulation of wakefield depicting the trailing electrostatic field in red, electron density in blue, and the driving laser pulse in yellow. The clear coherency due to the high phase velocity (in fact relativistic) wakefields is demonstrated (from [136]).

Inspired by spatially pinpointed, and temporal coincidences in various emission types from sources possessing jets, a quantitative comparison of the observational features mentioned in the previous sub-chapter is done using a wakefield acceleration (WFA) model layed out in Ch. 2, a mechanism that can readily give rise to such characteristics [46, 47]. This endeavour has already garnered interest from the broader scientific community [77, 67] as a new acceleration mechanism potentially capable of shedding light on the mystery that are UHECRs in addition to coincidental GRBs and neutrino events. It is argued that the compact central objects (active galactic nuclei, or active stellar binaries) can accompany accretion disk and jets [129, 135, 35]. Under these circumstances, in spite of the disparate central masses among the selected objects, similar physical sequences and observational features may be expected. The structure and dynamics, we study in theory and find in observations, lead to unique and characteristic spatial, temporal and energetic features. It will be shown that many of the various emission signals observed are in fair agreement with their corresponding predicted values. However, foregoing providing accurate analyses of

UHECR flux we might expect to see from Earth for each particular source. This is because intergalactic magnetic fields, the angle between our line of sight (LOS) and the polar axes of the accreting object, and the power-law index, p, that determines the rate of spreading for a given source's jets (see appendix A) all heavily factor into providing an accurate estimation of the flux one might expect to arrive at Earth. Instead we opted to report the total values, as if an observer were to capture all of the emitted UHECRs. Other acceleration mechanisms, such as first-order Fermi shock acceleration [29, 28], magnetic reconnection [41, 39, 122], and turbulent heating/acceleration [109] are contrasted with the present model.

A charged particle can be trapped by a plasma wave (wakefield), and thus accelerated only if its velocity is within the trapping velocity width of the wave, $v_{tr} = \sqrt{qE/mk}$, where E is the electrostatic field created by the plasma wake, k is the wavenumber, and q and m are the charge and mass of the particle, respectively [108]. Typically $v_{ph} \gg v_{th}$ when exciting wakefields, where v_{ph} is the phase velocity of the wave, and v_{th} is the thermal velocity of the plasma. Otherwise, if $v_{ph} \sim v_{th}$, then the wave is resonant with the bulk plasma and instabilities such as the drift wave instability can occur and the wakefield becomes unstable [136]. When the wave is intense enough such that $v_{tr} \sim v_{ph} \gg v_{th}$ the wakefield traps the bulk of the plasma and is stable. We also note that in addition to the particle acceleration vector being parallel to the electrostatic wave vector, the acceleration gradient is constant in time (before the wave begins to dissipate) and Lorentz invariant, making WFA very efficient (see Fig. 1.2).

In a typical young star-forming galaxy with an AGN, the rotational plasma motion around the AGN amplifies the embedded magnetic field of the disk leading to large accretion events [25, 91, 46]. This accretion is followed by the Shibata & Uchida [128] MHD propulsion of the accretion jets with a remarkable structure formation, whose relativistic factor of the jet motion, Γ, may be as large as 10^3. Such jets can exhibit a huge spatial extent and structural integrity over 10 - 10^3 times the accretion disk diameter. Typically, the well collimated,

narrowly defined jets show a clean and undisturbed structure, suggesting that such highly relativistic dynamics shields itself from rapid turbulence and destruction of the jet structure. (After a long propagation and emanation of its energy, the jet begins to deplete, and then the jet motion starts to interact strongly with the surrounding intergalactic plasma, forming cocoon-like swollen clouds of plasma instabilities as seen at the end of each jet in Fig. 1.2). We consider intense wakefield formation in these jets, triggered by the episodic events of large bulk accretion driven by the magnetorotational instability (MRI) [25] process in the accretion disk [91], which can cause a large pulse of shear motion of the magnetic fields at the root of the plasma jet [46]. We find from our estimate that the induced wakefields normalized intensity, $a_0 \equiv qE/m\omega c$, is as large as 10^{10} (ultra-relativistic regime of wakefield acceleration; [136]), which implies $v_{tr} \approx c$. In general, the greater the relativistic intensity (i.e. a_0) is, the stronger are the coherence and integrity of the wakefields [133]. Therefore, we expect that the resultant wakefields can persist over quite a large spatial extent within the jets without quickly depleting its energy. The Alfvén speed, v_A, in a jet is nearly equal to the speed of light due to the generally very strong magnetic field and low plasma density. Since $v_{tr} \sim v_{ph} = v_A \gg v_{th}$, the condition is met for stable acceleration of the bulk plasma in a jet.

1.4 Accretion disk Dynamics

The starting point of the present model for wakefield acceleration of UHE particles in AGN jets utilizes Shakura & Sunyaev's (S&S) analysis of accretion disk structure from their seminal paper on the topic [126], with an inclusion of a modified orbital resistivity, α (see 1.5), due to the resistivity of sheared magnetic fields. The following assumptions are made in order to obtain a steady-state, closed system of equations for the disc's thickness $2z_d$, density ρ_d, and internal energy ε_d: disk is axisymmetric and geometrically thin, hydrostatic equilibrium in

the z-direction, rate of accretion of matter is constant, and angular momentum is conserved. This allows one to obtain the accretion rate

$$\dot{M} = \dot{m}\dot{M}_c = \frac{2\pi c R_0}{3\epsilon\kappa_T}\dot{m}m, \tag{1.3}$$

where $\dot{M}_c$ is the critical accretion rate at the Eddington limit [124], and radiation luminosity of the disc

$$L_{rad} = \frac{4\pi c G M_\odot}{\kappa_T}\dot{m}m, \tag{1.4}$$

in terms of fundamental parameters, and simply the mass of the central accreting object, m (normalized by the solar mass constant $\mathrm{M}_\odot$). c is the speed of light, $R_0 \equiv 6GM_\odot/c^2$ is the ratio of the innermost stable circular orbit and m, ϵ is the radiation efficiency of the accretion disc, and κ_T is the opacity for Thomson electron scattering. Notice, $\dot{m}$, can be evaluated using observational estimates for the radiation luminosity and mass – this will be useful later on when estimating final values.

Famously, S&S found that their evaluation of the fluid dynamic resistivity was roughly two to three orders of magnitude smaller than observational estimates. Decades later, Balbus and Hawley's analysis of the MRI of accretion disc's demonstrated the significance of magnetic resistivity in accretion disk dynamics [25]. Matsumoto and Tajima's evaluation for the magnetic resistivity

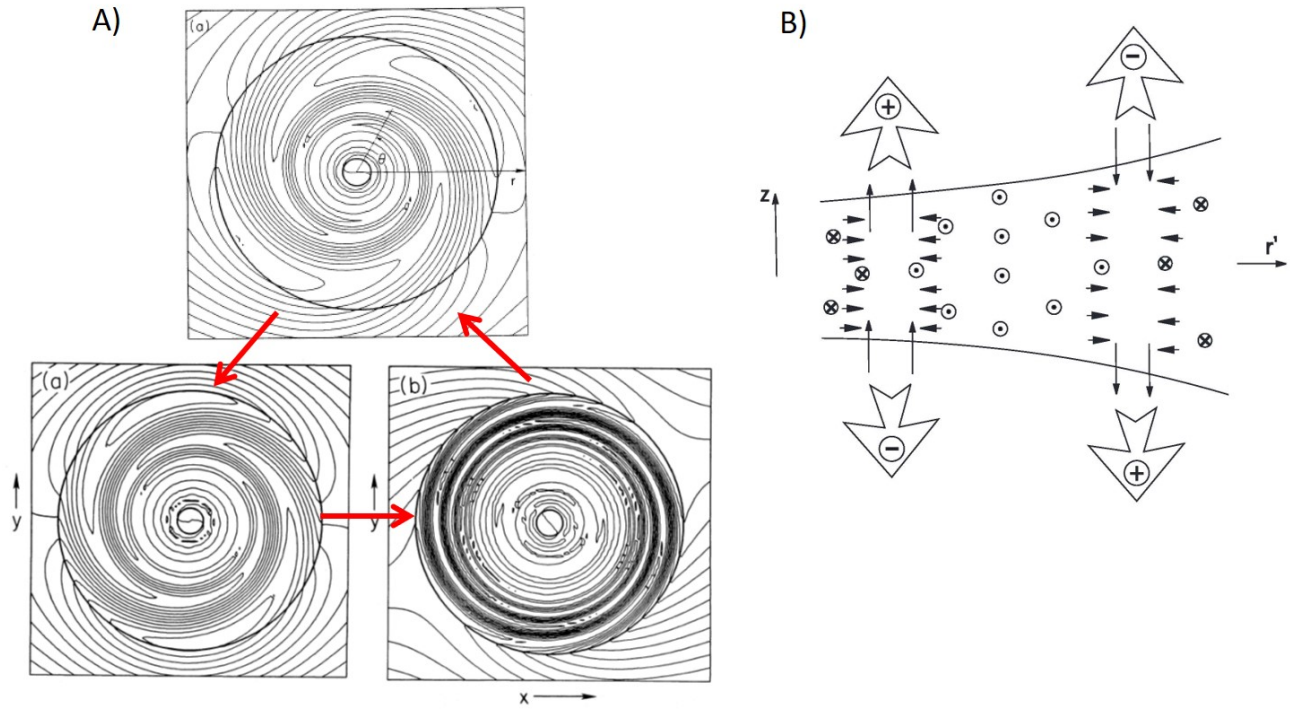


Figure 1.4: The physical consequences of the magneto-rotational instability. A) Magnetic field is amplified by the winding motion due to the differential rotation of the accretion disk. When the field strength becomes too resistive for the accretion disk to maintain steady-state Keplerian rotation, a sudden, massive accretion event occurs, causing the field to snap back to the less magnetized state, emitting an Alfvénic burst as a result (from [55]). B) Magneto-Rotational Instability (MRI) produces an electro-static field, which accelerates charged particles and heats up the disk halo. They eventually produce low energy photons in keV-MeV energy range (from [63]).

$$\alpha = \frac{\langle \delta B^2 \rangle}{12\pi\rho C_s^2} = \frac{1}{3\langle \beta \rangle} \tag{1.5}$$

is used in the present model [91], where $\langle \delta B^2 \rangle$ is the time-averaged magnetic fluctuations, and β is the usual ratio of thermal plasma energy to magnetic energy. This resistivity parameter will reappear in later formulae that are dependent on density, and internal energy of the accretion disc.

Balbus & Hawley found in their analysis that a negative angular velocity gradient (as is always the case in a accretion disk – differential rotation) in combination with any small seed field *always* leads to dynamic instability. This is due to the inevitable shearing of the azimuthal magnetic field, causing the resistivity to increase, disturbing the otherwise steady-state orbit of the disc. The magnetic fields grow until $\beta \sim 1$. This implies the maximum value of α is approximately 1/3, which on the order of observational estimates of 0.1 – 0.01. The growth rate of the MRI is on the order of several rotational periods. The critical wavelength of the instability is

$$\lambda = \frac{v_A}{C_s}\frac{\Omega}{A}z_d = \frac{R_0}{\sqrt{6}\epsilon}\alpha^{1/2}\dot{m}m, \tag{1.6}$$

which is assumed to be the wavelength for the Alfvén wave excited by the eruption of the disk [25]. v_A is the Alfvén speed ($\sim c$), Ω the orbital angular velocity (evaluated at the innermost stable orbit in the present case), C_s is the sound speed, and A is the Oort constant of the disc. The frequency of the wave is therefore

$$\omega_A = \frac{2\pi c}{\lambda} = \frac{2\sqrt{6}\pi\epsilon c}{R_0}\frac{1}{\alpha^{1/2}\dot{m}m}. \tag{1.7}$$

Large *clumps* of matter form in the areas of the disk where the field is weaker (see Fig. 1.4), falling out of equilibrium with the gravitational pull of the central accreting object, leading to violent eruptions of the disk when said clumps accrete onto the SMBH (or NS). (See Fig. 2.1). Angular momentum is transported outward to the "second ring," which then moves outward [25], and is therefore conserved.

We now consider the likely scenario that electromagnetic pulses are produced in the jets near the innermost part of the accretion disk. When large amounts of matter suddenly accrete onto the central compact object, the magnetic field at the base of the jet is perturbed, creating an extremely intense Alfvénic-type wave capable of accelerating charged particles to very high energies by electromagnetic wave-particle interaction via wakefields [134]. The episodic, eruptive accretion from the disk caused by the MRI [25] can give rise to such strong electromagnetic pulses, which act as the drivers of the collective acceleration of the pondermotive force. The pondermotive force drives the electrostatic wakes that follow behind, similar to a duck or boat creating a wake behind it as it moves through the water, which trap and accelerate protons. The accelerated protons are released to the intergalactic space and some eventually reach, and decay in Earth's atmosphere as cosmic rays. Some of them collide with slower protons in the jet, or gaseous lobes to produce secondary particles, such as neutrinos and gamma-rays. The high-energy electrons, on the other hand, driven by the pondermotive force in front of the seed wave emit photons as a result of their orbits, and from collisions with electromagnetic perturbances, to produce various non-thermal emissions (radio, IR, visible, UV, and gamma-rays).

Blandford and Payne's [31], and Blandford and Znajek's jet models [32] are steady-state, ideal MHD theories that focus on local magnetic fields. An important implication from these theories is that jets are born magnetically dominated and therefore there must be a process or processes that convert this magnetic energy into kinetic energy. WFA may be one such process, and would also explain the long, coherent structure of jets given the increased stability at relativistic intensities [136]. Our theory, assumes a constantly evolving, fluctuating, global magnetized accretion disk (see Fig. 1.4). The triggering of an Alfvénic burst that excites a wakefield is dependent upon global (entire disk) magnetic field instabilities. When a global magnetic field is present in a Keplerian rotating accretion disk, Balbus-Hawley type instabilities (MRI) are unavoidable. Matsumoto and Tajima [91] showed the beta parameter can vary from ~ 100 to ≤ 1 in the accretion disk (also see eqn. 4.32, 4.28 in Ref. [135])

due to the MRI. Furthermore, jet formation requires a global field theory [63, 135, 129, 25]. The strength of the magnetic field and the size of the perturbation, which depends on the black hole mass, dictate the intensity of the Alfvén wave, similar to how the magnetic reconnection power scales with the mass of the black hole [130, 74]. The beta and magnetization parameters of the accretion disk may indirectly affect the intensity of the waves and how frequently they are launched, but fine tuning of model parameters can account for this and the physics remains the same, as will be shown.

The dynamics of ultra-relativistic WFA are distinct from magnetic reconnection (MR). MR accelerates particles via the magnetic component of the Lorentz force in magnetic discontinuities. In WFA it is the pondermotive force of the electromagnetic wave that drives electrons ahead of the wave. The wake, a depression in the plasma density behind the wave, traps positively charged particles that are accelerated by the electrostatic pull of the cluster of electrons ahead of them [134]. MR and WFA would occur in different parts of the AGN-jet system. MR can occur in the accretion disk and in the jet before it becomes kinetically dominant [95], at which point WFA is strongest. WFA occurs solely in the jet and the acceleration direction is always parallel to the wave vector, unlike MR. The latter point is important to realize since this may imply isotropic emission of UHE particles from MR, in contrast to observations (see Fig. 3.1). The wakefield traveling along the jet can remain coherent and accelerate particles virtually the entire length of the jet [46].

It should also be mentioned that MR plays an important role in disk-jet evolution in addition to particle acceleration. E. M. de Gouveia Dal Pino *et al.* showed that violent MR of the the jet and disk fields accelerates and injects particles from the disk into the jet [41, 40]. Also, Nishikawa *et al.* showed that at larger scales kinetic instabilities in the jet plumes can drive MR and is capable of accelerating electrons and protons [106]. MR and MRI are intimately related, likely occurring together or sequentially. The accretion disk must fluctuate magnetically due to Keplerian twisting of the disk fields, stretching field lines until

the magnetic resistivity is great enough that matter accretes onto the black hole and then snaps back to its original state. Once the field strength has reached it's threshold, magnetic energy is released via MR and intense Alfvénic pulses (like a rubber band snapping back to it's relaxed state), which subsequently heats the disk corona, launches particles into the jet and accelerates them. While MR [95, 39, 106] and shocks [94] are capable of accelerating particles to ultra-high energies, we will argue in the following chapters that WFA may be responsible for the generation of the majority, and most energetic UHECRs, given it's ease at coherently accelerating ultra-relativistic charged particles over parsec to kilo-parsec scales depending only on the mass of the central accreting object in galactic and extragalactic sources possessing jets.

Before we close this chapter, let us mention a separate, but important associated result of the recent simultaneous observation of the gravitational waves [101] and gamma rays from the collision of two neutron stars [5, 6]. When LIGO observed the gravitational wave (GW) arrival [6]. It was suggested [137] that a collision of two neutron stars can yield not only the emission of violent phenomena such as GWs, but also gives rise to the formation of an accretion disk and its jets. It follows that an eruption at the base of the jets, such as a massive accretion, produces wakefield acceleration of electrons (and thus gamma rays), following the emission of a GW. Thus, we see that the gamma ray emission is an important indicator of the underlying physical process of the electron acceleration (by WFA) and alerts us to the importance of the multi-messenger astrophysics approach.

Chapter 2

Wakefield Acceleration in Jets

The emerging new mechanism of wakefield acceleration of [134] has quite a different theoretical construct in contrast to a stochastic acceleration mechanism. It is based principally on a single astrophysical object such as an AGN and its accretion disk and associated jets. An accretion disk instability, such as the MRI, can introduce the rapid increase of the present magnetic fields in the disk, which triggers episodic disruption of the accretion disk and subsequent disturbances at the feet of the jets [102, 55]. See Fig. 1.4. This disturbance may be considered as the trigger of intense electromagnetic (originally Alfvénic shock) pulses in the jets. The basic physical parameters of WFA in AGN jets are evaluated.

In the WFA theory, developed by T. Ebisuzaki and T. Tajima [46, 47], input parameters are m and $\dot{m}$. The former, m, the BH mass, normalised by the solar mass ($M_\odot = 2.0 \times 10^{33}\,\mathrm{g}$), can be estimated by observations such as stellar dynamics, QPO/recurrence period, and Eddington limit. The latter is the accretion rate, $\dot{m}$, normalised by the critical accretion rate, $\dot{M}_\mathrm{c} = 2\pi c R_0/3\epsilon\kappa_\mathrm{T}$, where κ_T is the Thomson scattering opacity and $\epsilon = 0.06$ is the radiation efficiency of the disk. The non-dimensional accretion rate $\dot{m}$ can be calculated using the radiation luminosity given by Eqn. 1.4, which is proportional to the product of $\dot{m}$

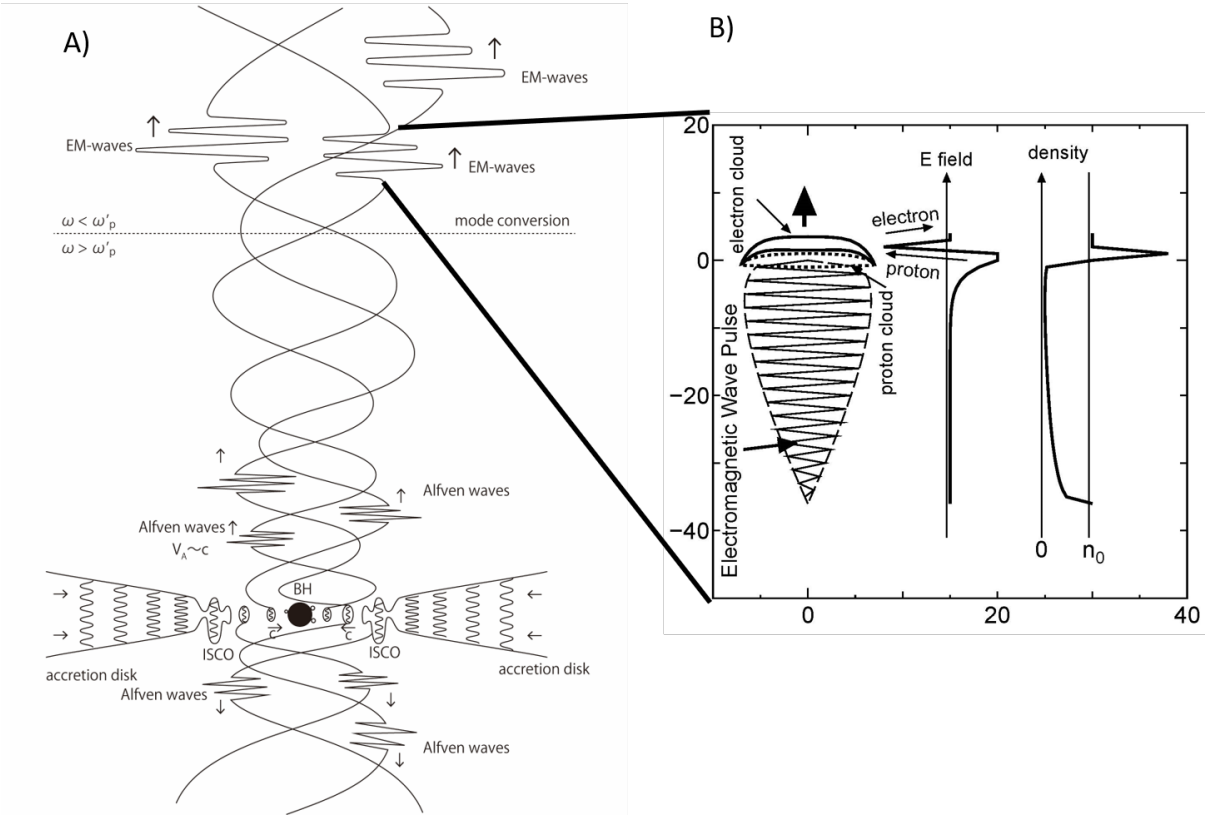


Figure 2.1: WFA theory for the accreting black hole-jet system of an AGN (from [67]). A) The cross section of an AGN, its accretion disk and jets. Alfvén waves generated upon large mass accretions at the base of the jet propagate along the field line of the jet. They eventually mode-convert into intense electromagnetic waves when the wave frequency matches the local plasma frequency, $\omega'_{\rm p} = (4\pi n_{\rm jet} e^2/m_{\rm e}\gamma\Gamma^3)^{1/2}$, where γ is the Lorentz factor of a trapped particle, and Γ is the bulk Lorentz factor of the jet. B) The structure of the bow wake. An electron cloud is formed at the front (top) of the wave pulse and a proton cloud follows. The resultant electric field accelerates protons in the back side and electrons in the front side of the bow wake. Since this acceleration structure moves at a velocity close to the speed of light, the charged particles with the same velocity (light velocity) in the field are accelerated for a long time and distance.

and m. The radiation luminosity $L_{\rm rad}$ can be estimated by emission lines from the nucleus for the case of active galactic nuclei (blazars, radio galaxies, and Seyfert galaxies) or by the X-ray luminosity for the case of less massive black holes ($< 1000 M_\odot$: intermediate and stellar mass blackholes). Since X-rays are believed to be emitted directly from the accretion disk by thermal mechanisms (not necessarily from the jets by non-thermal mechanisms) in the less massive blackholes, their anisotropies are minimal compared with those of gamma rays.

When m and $\dot{m}$, or equivalently $L_{\rm rad}$ are given, WFA theory predicts the rise time $2\pi/\omega$ of the burst, the episodic recurrence time $1/\nu$, and the acceleration time D_3/c, as follows:

$$2\pi/\omega = \frac{R_0}{6\epsilon c}\alpha^{1/2}\dot{m}m, \tag{2.1}$$

$$1/\nu = \frac{\sqrt{6}R_0}{c}\alpha^{-1/2}m, \tag{2.2}$$

$$D_3/c = \frac{1}{36}\left(\frac{e^2 R_0^4}{4\pi^3 c^5 m_{\rm e}^2 \epsilon^5 \kappa_{\rm T}}\right)^{1/3} \alpha^{5/6}\dot{m}^{5/3}m^{4/3}, \tag{2.3}$$

where $R_0 = 6GM_\odot/c^2 = 9.0 \times 10^5\,{\rm cm}$ is the radius of the innermost stable orbit of a one solar mass black hole, c the light velocity, α the disk-resistivity parameter [126], e and $m_{\rm e}$ are the electron charge and mass, respectively. Note that we have assumed a value of $p = 0.5$ for the power-law jet-spreading index in our formulation (see appendix A). This value can be adjusted on a per-source basis to obtain a more accurate model, however, due to lack of accurate data on jet angles this value is adopted in the analysis of each source.

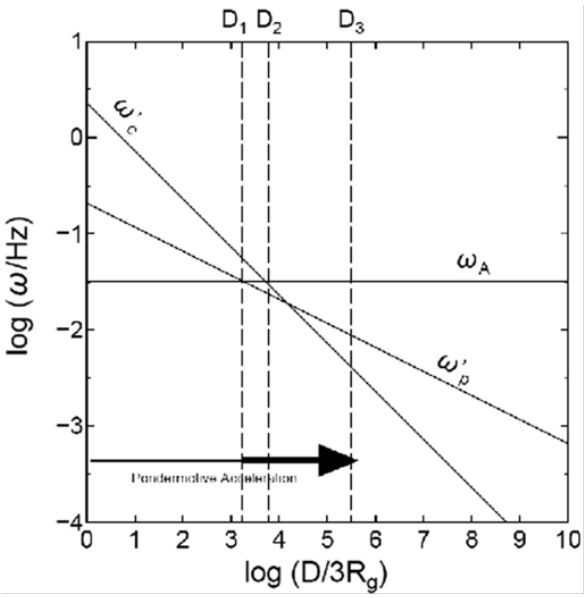


Figure 2.2: Plot of frequencies versus distance from the accretion disk normalized by the radius of the innermost stable circular orbit, where log here is base 10 (from [46]). The frequency of the emitted Alfvén wave $\omega_{\rm A}$, relativistic plasma frequency $\omega'_{\rm p}$, and relativistic electron cyclotron frequency $\omega'_{\rm c}$ are shown. When the (orginally of Alfvénic type) wave reaches the overdense plasma $\omega_A > \omega'_p$ it mode converts to a more typical electromagnetic wave, and wakefield acceleration occurs, if not before then.

Protons are accelerated in the back side of the bow wake (see Fig. 2.1B). The maximum proton energy (i.e. UHECR) is obtained by integrating the pondermotive force of the longitudinally polarized electrostatic wake $F = z\Gamma m_e c a \omega$ (see Fig. 2.2), for a particle with charge z, where a is the Lorentz invariant vector potential of the wave, and Γ is the bulk Lorentz factor of the jet.

$$W_{\rm max} = \frac{1}{9}\left(\frac{e^4 c^2 R_0^2}{2 m_e \epsilon^4 \kappa_{\rm T}^2}\right)^{1/3} z\Gamma \alpha^{2/3} \dot{m}^{4/3} m^{2/3} \tag{2.4}$$

See Fig. 2.3.

The luminosity of UHECR is calculated as:

$$L_{\rm UHECR} = \frac{\zeta \sigma \alpha^{1/2}}{6\epsilon} L_{\rm rad}, \tag{2.5}$$

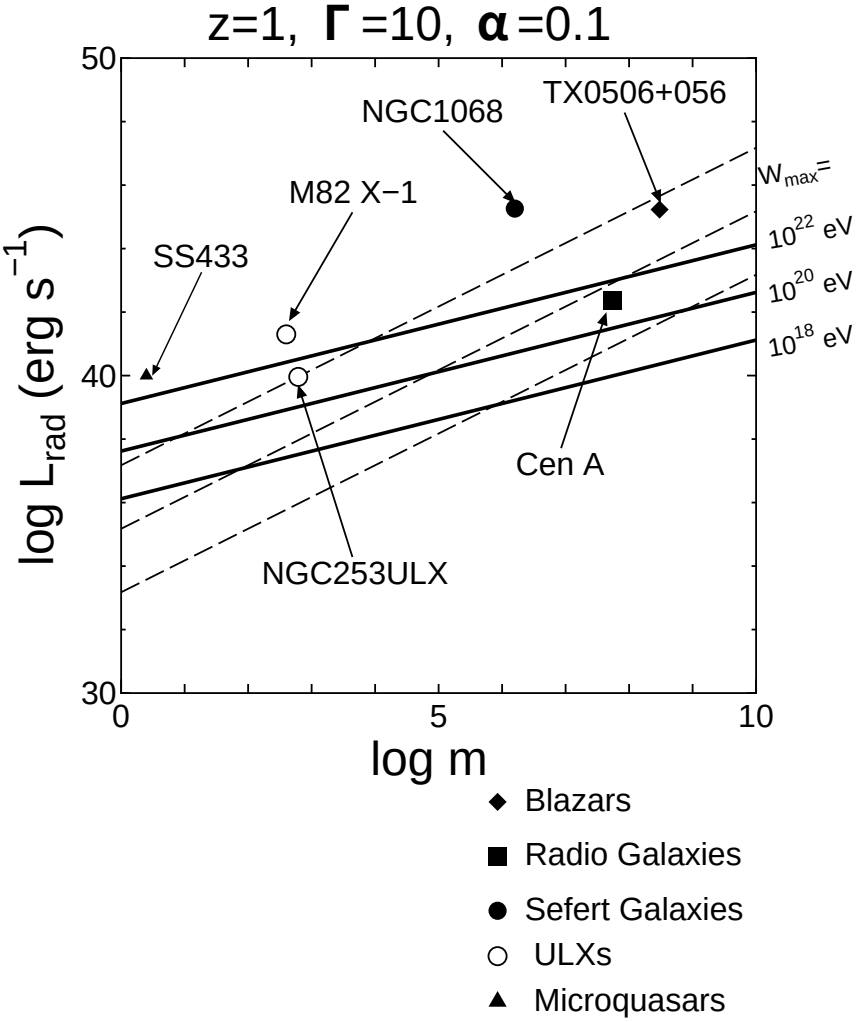


Figure 2.3: The maximum energies of protons, $W_{\max}$, are predicted using the mass of the central black hole (normalized by one solar mass), m, on the right abscissa, and total radiation luminosity, $L_{\rm rad}$, by the wakefield acceleration theory [136] on the left abscissa. Various astronomical objects, such as microquasars ($m = 1 \sim 10$), ultra luminous X-ray sources (ULXs; $m = 100 \sim 10000$) in starburst galaxies, central blackholes of Seyfert galaxies $m \sim 10^6$ and radio galaxies/blazars ($m = 10^7 \sim 10^{10}$) can accelerate UHECRs with energy above 10^{20} eV. The individual points (or boxes) are plotted based on their known (or estimated) central mass according to our theory. Here, we assume the charge is $z = 1$, the bulk Lorentz factor of the flow of the jets $\Gamma = 10$, and $\alpha = 0.1$ the "α" parameter of the disk. From top to bottom, the three dashed lines represent $\dot{m} = 10^{-1}$, 10^{-3}, and 10^{-5} (from [67]).

where σ is the energy efficiency of the charged-particle acceleration, including the conversion of Alfven wave into electromagnetic waves, and

$$\zeta = \frac{\ln(W_{\max}/W_0)}{\ln(W_{\max}/W_{\min})}. \tag{2.6}$$

Here, $W_0 = 0.57 \times 10^{20}$eV.

On the other hand, the electrons are accelerated in the front side of the bow wake (Fig. 2.1B), simultaneously with protons behind. The accelerated electrons emit high energy gamma-rays with the energies ranging GeV-PeV due to the collision with the magnetic perturbations.

The luminosity of gamma-rays is given as:

$$L_\gamma = \frac{\sigma\alpha^{1/2}}{6\epsilon} L_{rad}. \tag{2.7}$$

For the reader's convenience, we summarize the scaling laws represented by the equations above in Table 2.1.

The UHECR flux at Earth is calculated as:

$$F_{\rm UHECR} = 6.7 \times 10^{-1} \left[\frac{\rm UHECRs}{100\ \rm km^2 yr}\right] \left(\frac{d}{3.6\rm Mpc}\right)^{-2} \left(\frac{L_{rad}}{10^{42}\rm ergs^{-1}}\right) \tag{2.8}$$

for the case of iostropic radiation with $\ln(\mathrm{W_{max}/W_{min}}) = 30,\ \alpha = 0.1,$ and $\sigma = 0.1$.

Ultra-high-energy protons, accelerated by the wakefield, may collide with another proton in the plume of decelerated material in the jet or interstellar gas near to produce pions, which

decay into gamma rays, electrons, and neutrinos. The neutrino flux at Earth, F_ν, can be obtained from,

$$W_\nu^2 F_\nu = \frac{f_{pp}\sigma\alpha^{1/2}L_{rad}}{6\Omega d^2\epsilon \ln W_{\max}/W_{min}} \tag{2.9}$$

where f_{pp} is the collision probability of protons, Ω is the solid angle of the emission ($\Omega = 4\pi$ for the isotropic case) and we assume $W_\nu = 0.05W_p$, where W_p is the same as $W_{\max}$.

It may be possible that the angle at which the jet spreads out from the central accretion object alters these parameter values. Such an assumption is not made in the present model nor in our results, however, we have included alternate formulas for an arbitrary value of p in appendix A.

Table 2.1: Time Scales, Maximum Energy, and Luminosities estimates (see Huxtable *et al.* [67])

Quantities	Scaling Laws	Units	Equation Numbers
$2\pi/\omega$	$8.2\times10^{-5}\alpha^{-1/2}\dot{m}m$	s	2.1
$1/\nu$	$7.3\times10^{-5}\alpha^{-1/2}m$	s	2.2
D_3/c	$1.7\times10^{2}\alpha^{5/6}\dot{m}^{5/3}m^{4/3}$	s	2.3
$W_{\max}$	$3.2\times10^{-31}z\Gamma\alpha^{2/3}m^{-2/3}L_{\rm rad}^{4/3}$	eV	2.4
$L_{\rm rad}$	$1.5\times10^{38}\dot{m}m$	erg s^{-1}	1.4
L_γ	$2.78\sigma\alpha^{1/2}L_{\rm rad}$	erg s^{-1}	2.7
$L_{\rm UHECR}$	$2.78\sigma\zeta\alpha^{1/2}L_{\rm rad}$	erg s^{-1}	2.5

We have seen that the rotating accretion disk accompanied by the magnetic fields emanates

well-collimated extended jets that are wrapped by helical magnetic fields. These astrophysical jets are one of the largest structured of the Universe (see Fig. 1.2). This structure, as has been observed in many astrophysical objects, is also accompanied by additional structured entities in it, such as the formation of wakefields that propagate through the jets. First, the presence of the magnetic fields in the jets allows the disturbances (Alfvén shocks) from the accretion disk to propagate in the plasma due to the physical properties of the electromagnetic waves in the plasma. This allows the EM disturbances created at or near the accretion disk to propagate through the [otherwise evanescent ($\omega > \omega_p'$)] plasma to its accelerating range ($\omega > \omega_p'$). Thus, the presence of the magnetic field in the jets acts as a conduit for these intense EM disturbances that may be created by the accretion disk.

The created intense EM waves (due in part to their highly relativistic dynamics) often have highly relativistic group velocities. As has been discuessed above, the EM waves with high group velocity are capable of creating an intense longitudinal plasma wave structure, whose phase velocity is also relativistic (close to c), in other words a wakefield. It has been shown and demonstrated (experimentally and theoretically) that these wakefields generated with high phase velocity is close to the speed of light, by far, much greater than the the thermal velocities of the bulk plasma, so the plasma remains quite stable and the excited waves remain robust. In other words, by the time the plasma electrons repond to the wakefield's electric fields, with the elctron speed less than c, the waves have escaped away from the responding electrons, thus keeping these high-amplitude plasma waves in tact.

It remains robust also due to the fact that all electrons in this regime, even while responding to the high phase velocity, can move at (or near) the speed of light, which is in fact the speed at which the wakefields are moving, so these electrons, in fact, can reinforce the movement of the wakefields. This is called relativistic coherence [136] and is the reason why the wakefields themselves are stable and robust, in addition to the robustness of the observed astrophysical jets.

We see that the astrophysical jets only eventually begin to form lobes at their ends when the particles that propagate through the jets have now expended their energies to become weak enough to interact with the bulk plasma strongly where a variety of plasma instabilities may take place.

As discussed above, the conditions for strong acceleration by wakefields are:

(a) the acceleration structure (wave) is very close to the relativistic propagation velocity (phase velocity), i.e. the speed of light; and

(b) the wave has a relativistic amplitude (i.e. the particles in the wave have relativistic momentum $e_j E/\omega > m_j c$ in one photon cycle, where e_j and m_j are the charge and the mass of the particle j, and E and ω are the electric field and angular frequency of the wave, respectively).

We applied the above WFA model to six candidates from a broad range of central black hole (BH), or neutron star (NS) mass. In this chapter we first derive the formulae used in our predictions, then in the proceeding chapter each case study is presented in descending order of mass: blazar TXS 0506+056, radio galaxy Centaurus A, Seyfert galaxy NGC 1068, starburst galaxies M82 and NGC 0253, and finally microquasar SS 433. We survey and scrutinize general commonalities as well as specific characteristics of their various signals, including cosmic-rays and UHE gamma rays. Localized UHECRs or neutrinos have been observed in all cases, except SS 433. These six astrophysical objects have vastly different central masses from $\sim 10^9$ down to only several solar masses. Nonetheless, their polar jets exhibit common phenomena of intense acceleration, and in a fundamentally linear fashion with a pulsed operation given the episodic motion associated with the central object's accretion disk [25, 55]. Thus, the direction of arrival of UHECRs is localized (anisotropic) as well as accompanied by gamma-ray emission (due to the electron acceleration) with a specific separation in the arrival time of the signals. Neutrino arrival may be coincidental, but

delayed in time as well. In other words, though the mass scales differ vastly, the underlying mechanisms are remarkably common; the burst periods and rise and fall times may differ among cases, but the mass dependence and qualitative features are curiously common. This is what we wish to investigate in detail for our six astrophysical objects. The emerging picture is a surprisingly unified, integrated physical mechanism of wakefield acceleration.

Chapter 3

Test Cases

In each of the following sub-chapters, and single source that is known (or shows strong evidence) to possess jets is surveyed. Six different sources in total, ranging in central accreting object (SMBH or neutron star) mass from $\mathcal{O}(1)$ to $\mathcal{O}(10^8)$ $M_\odot$, are scrutinized on their probability to be significant sources of UHECRs as well as ultra-high energy (UHE) gamma-rays and neutrinos. A candidate *likely* to produce detectable UHECRs was chosen from several different classes of objects: blazar, radio galaxy, Seyfert galaxy, starburst galaxy (M82 & NGC 253), and microquasar. This was done to illustrate the unifying power of WFA theory in explaining not only the emitted signals, their temporal and spatial variability, but also the structural similarities of blazars, microquasars and every system in between that exhibits jets.

3.1 Blazar: TXS 0506+056

TXS 0506+056 in constellation Orion is a blazar with a redshift of 0.3365 ± 0.0010 [111], which corresponds to about 1.75 Gpc from Earth. TXS 0506+056 was first cataloged as

a radio source in 1983 [82], and then confirmed to be a blazar [89]. Gamma-rays emitted from TXS 0506+056 were detected by the EGRET and *Fermi*-LAT missions [80, 62, 8]. In addition, radio observations have shown apparent superluminal motion in the jet [120].

On 22 September, 2017 the IceCube Neutrino Observatory detected high-energy neutrinos coming from a direction consistent with this flaring gamma-ray blazar TXS 0506+056 [69]. The most probable energy for the observed neutrino is around 190 TeV with a 90% confidence level, and lower limit of 183 TeV, depending only weakly on the assumed astrophysical energy spectrum. This suggests the existence of high-energy protons or nuclei with tens of PeV generated in the jet of the Blazar. The detection of high energy neutrinos suggests charged particles are accelerated parallel to the jet axis.

During approximately 2 weeks of the neutrino observation, a peak flux of gamma-ray emission around $5.3 \times 10^{-7}\,\mathrm{cm}^{-2}\,\mathrm{s}^{-1}$ is also reported by *Fermi*-LAT, with an energy range between $0.1 \sim 100$ GeV [68]. The associated isotropic luminosity during the period reaches as high as $1.2 \times 10^{47}\,\mathrm{erg\,s}^{-1}$[69]. Analysing the data prior to the event, a long-term isotropic gamma-ray luminosity between 0.1 GeV and 100 GeV is derived with an averaged value of 0.28×10^{47} erg/s over 9.5 years of *Fermi*-LAT observations of TXS 0506+056 [69]. According to their study, the neutrino emission coincides with a peak in very high energy (VHE) gamma-ray flux and a local minimum of the spectral index (Fig. 1 of [68]), which is similar to fluctuations of the spectral index caused by the MRI as depicted in Fig. 7 in [34].

The coincidental detection of high energy signals encouraged us to test WFA as an alternative explanation. According to the WFA theory, the relativistic pondermotive acceleration in the jet can boost particles to an energy over ZeV [46, 47, 136]. Also, because the particles are accelerated linearly, the corresponding signal detected can be highly beamed and emitted axially from the jets. In the rest of the chapter, we will estimate several physical parameters using our WFA model and compare them with their analogous observational value.

Mass estimation is difficult in general for blazars. Padovani *et al.* [110], however, estimated the central black hole mass to be $3 \times 10^8\, M_\odot$ using the relations of black holes mass and R-band bulge magnitude $M(R) \sim -2.9$ [112, 111], assuming the host galaxy to be a giant elliptical. The bolometric luminosity ($\simeq L_{\rm rad}$) of $1.7 \times 10^{45}\,{\rm erg\,s^{-1}}$ takes into account the over estimation due to the jet-induced component of the bolometric luminosity derived from the OII and OIII lines ($L_{\rm OII} = 9 \times 10^{45}\,{\rm erg\,s^{-1}}$ and $L_{\rm OIII} = 3 \times 10^{45}\,{\rm erg\,s^{-1}}$), respectively. Substituting $m = 3 \times 10^8$ and $L_{\rm rad} = 1.7 \times 10^{45}\,{\rm erg\,s^{-1}}$ into equations 2.4, 2.1, and 2.2, we derived $W_{\rm max} = 3.1{\times}10^{24}{\rm eV}$, $2\pi/\omega = 3.0{\times}10^3\,{\rm s}$, $1/\nu = 6.9{\times}10^4\,{\rm s}$, and $L_\gamma = 1.5{\times}10^{44}\,{\rm erg\,s^{-1}}$, as shown in Table 3.1.

Greisen, Zatsepin and Kusmin (GZK) [59, 145] showed that UHE protons traveling through the cosmic microwave background will undergo inelastic collisions with photons, limiting the maximum energy of UHECRs that traveled 100 Mpc to 10^{20} eV. If this distance is shorter, however, the attenuation is less, and the opposite is true if the source is farther away. Given the distance between the source and Earth, the attenuated maximum energy can be calculated. This *attenuated* value for W_{max} can then be substituted into eqn. 2.6 to obtain a more accurate prediction of UHECR flux and luminosity that terrestrial observers might detect. We have not accounted for this effect in our calculations, because there are additional factors that can reduce the energy and flux of UHECRs and they are difficult to account for. We have already mentioned the jet-spreading index p and the anisotropy of UHE particles emitted from jets, but extragalactic magnetic fields and gaseous clouds also attenuate UHECR luminosity.

According to the MAGIC observation [22] VHE gamma-rays, above 90 GeV, from TXS 0506+056 varied, increasing by a factor of 6 within a day. We may set $2\pi/\omega = 4.8 \times 10^4\,{\rm s}$ or shorter as an e-raising time. There are two periods (3-4 October 2017, and 31 October 2017) of enhanced gamma-ray emission. We may set $1/\nu$ as $2.4 \times 10^6\,{\rm s}$ or shorter, taking into account the incomplete observation in TeV gamma rays.

The theoretical gamma-ray luminosity is calculated as $L_\gamma = 1.5 \times 10^{44}$ erg s^{-1} (see Eq. 2.7), which is much less than the observed isotropic gamma-ray luminosity $2.8 \times 10^{46}\,\mathrm{erg\,s^{-1}}$ observed by *Fermi*-LAT [69]. This is likely due to the under estimation of the total luminosity as a result of the large distance (1.75 Gpc) between us and the blazar.

If the actual emission is strongly beamed, assuming isotropic emission will overestimate the luminosity by integrating the whole sphere. If we assume a 10° angle of spread for the beam, the corrected estimation of the *Fermi*-LAT luminosity will be 2 orders of magnitude lower than their reported value. That is, $L_\gamma^{(10^\circ)} = 4.6 \times 10^{44}$ erg/s, which is consistent with the theoretical luminosity.

Here, W_ν, and W_p are the energies of the neutrino and the proton, respectively. Substituting $f_\mathrm{pp} = 1.0$, $L_\mathrm{rad} = 1.7 \times 10^{45}\,\mathrm{erg\,s^{-1}}$, d=1.8 Gpc, $\sigma = 0.1$, $\alpha = 0.1$, $\epsilon = 0.06$, $\Omega/4\pi = 4.8 \times 10^{-2}$ for $\theta = 10^\circ$, and $\ln(W_\mathrm{max}/W_\mathrm{min}) = 30$ into equation 2.9, we obtain $F_\nu = 8.1 \times 10^{-16}\,\mathrm{TeV^{-1}\,cm^{-2}\,s^{-1}}$ at 100 TeV. It is consistent within 50% of the observed flux by IceCube of $F_\nu = 1.6 \times 10^{-15}\,\mathrm{TeV^{-1}\,cm^{-2}\,s^{-1}}$ at 100 TeV [69].

WFA theory might explain the simultaneous arrival of high energy gamma-rays and neutrinos from blazars, because particles are linearly accelerated and would continue traveling along the jet's axis once emitted. Our WFA model gives an underestimated gamma-ray luminosity compared to the observational data. This discrepancy may be explained by the localization of the beam-like emission in contrast to the isotropic emission. The periodicity of neutrino bursts may be qualitatively explained by fluctuations of the magneto-rotational instability that trigger intense electromagnetic pulses, which accelerates protons to become UHECRs and produces VHE gamma rays. Although it can be difficult to detect the highest energy particles at present, future studies may find more evidence to support our theory.

Table 3.1: Comparison of observed parameters (shaded) and theoretical parameters (without shade). Taken from Huxtable *et al.* (2023) [67]. Theoretical and observational values for a range of astrophysical objects, including a blazar (BL), a radio galaxy (RG), a Seyfert galaxy (SyG), starburst galaxies (SBG) and a micro-quasar (MQ).

parameter	TX 0506+056	Cen A	NGC1068	M82	NGC 0253	SS 433
type	BL	RG	SyG	SBG	SBG	MQ
$\log d$ (pc)	9.24	6.53	7.15	6.56	6.54	3.54
$\log M_{\rm BH}(M_\odot)$	8.48	7.74	6.20	2.60	2.79	0.40
$\log L_{\rm rad}(\mathrm{erg\,s^{-1}})$	45.23	42.36	45.26	41.30	39.96	40.00
$\log W_{\rm max}$ (eV)	24.49	21.16	26.05	23.17	21.26	22.91
$\log L_{\rm UHECR}\,(\mathrm{erg\,s^{-1}})$	43.17	40.31	43.20	39.24	37.90	37.94
$F_{\rm UHECR}(/100\,\mathrm{km^2/yr})$	-	0.69	-	0.052	0.0026	-
$F_{\rm UHECR}(/100\,\mathrm{km^2/yr})$	-	0.016	-	0.040	0.013	-
$\log 2\pi/\omega$ (s)	3.47	0.62	3.50	-0.46	-1.81	-1.76
$\log 2\pi/\omega$ (s)	< 4.68	-	-	-	-	-
$\log 1/\nu$ (s)	4.84	4.10	2.56	-1.04	-0.85	-3.24
$\log 1/\nu$, (s)	< 6.38	4.18	-	-0.70	< 2.0	< 1.0
$\log L_\gamma\,(\mathrm{erg\,s^{-1}})$	44.17	41.31	44.20	40.24	38.90	38.94
$\log L_\gamma\,(\mathrm{erg\,s^{-1}})$	47.08	38.04	45.53	40.18	39.78	37.57

3.2 Radio Galaxy: Centaurus as A

Centaurus A (also known as NGC 5128), in constellation Centaurus, is a radio galaxy with kpc size jets, and is 3.4 Mpc from the Earth [70]. Cen A hosts an AGN (active galactic nuclei) believed to be a supermassive blackhole, whose mass is well defined by stellar dynamics [103] to be $m = 5.5 \times 10^7$. The radiation luminosity is also determined to be $L_{\rm rad} = 2.3 \times 10^{42}$ erg $\mathrm{s^{-1}}$ from X-ray observations [73]. Substituting the mass and radiation luminosity into equations 2.4, 2.1, 2.2, and 2.7 give us $W_{\rm max} = 1.4 \times 10^{21}$ eV, $2\pi/\omega = 4.2\,\mathrm{s}$, $1/\nu = 1.3 \times 10^4\,\mathrm{s}$, and $L_\gamma = 2.0 \times 10^{41}\,\mathrm{erg\,s^{-1}}$, as shown in table 3.1.

Our theory predicts that Cen A is capable of accelerating protons to energies above 10^{21} eV (see Table 3.1). If we assume isotropic emission of UHECRs, their predicted flux is $0.60\,/\mathrm{km^2}\,/\mathrm{yr}$. However, [1] observed UHECRs as energetic as 10^{20} eV arriving from the direction of Cen A (Fig. 3.1) with an observed flux of $0.016\,/\mathrm{km^2}\,/\mathrm{yr}$. As mentioned in the

previous sub-chapter, the large discrepancy in the perceived UHECR flux is likely due to the fact that the jets of Cen A are oriented nearly perpendicular to our line-of-sight (LOS), thus the vast majority of cosmic rays, especially the most energetic, ejected from its jets never reach Earth. Intergalactic magnetic fields may deflect some less-energetic protons towards Earth to become UHECRs. The episodic recurrence time predicted by our model is consistent with the observation of [53, 123], who detected fluctuating x-ray luminosity in the time scale of $10 - 20$ ks ($1/\nu \sim 1.5 \times 10^4$) (see table 3.1).

Cen A has been known to emit gamma rays in the range of TeV and greater for decades now. The H.E.S.S. telescope measured a gamma-ray flux of $0.45 \pm 0.07 \times 10^{-13}\,\mathrm{ph\,cm^{-2}\,s^{-1}TeV^{-1}}$ at 1 TeV (Fig. 4 in [17]) with a corresponding total gamma-ray luminosity of $1.1 \times 10^{38}\,\mathrm{erg\,s^{-1}}$ [61]. The factor of ~ 2000 difference between the theoretical and observational value for L_γ is again likely due to the fact that the axis of the jets are at a large angle to our line of sight (LOS), and naturally gamma-ray emissions are strongly beamed in the axially direction of the jets in the context of WFA.

3.3 Seyfert Galaxy: NGC 1068

NGC1068 is a Seyfert galaxy that has a bright nucleus with a central black hole of $1.6 \times 10^6\,M_\odot$ [58]. It is also undergoing an intense starburst process. It is located at a distance of 14 Mpc [140] in the constellation Cetus. A bolometric luminosity of the nucleus of $1.8 \times 10^{45}\,\mathrm{erg\,s^{-1}}$ was obtained from OIV line [58]. Substituting $m = 1.6 \times 10^6$, $L_{\mathrm{rad}} = 1.8 \times 10^{45}\,\mathrm{erg\,s^{-1}}$, and $\alpha = 0.1$ into equations 2.4, 2.1, 2.2, and 2.7 gives us $W_{\max} = 1.1 \times 10^{26}\,\mathrm{eV}$, $2\pi/\omega = 3.2 \times 10^3\,\mathrm{s}$, $1/\nu = 3.63 \times 10^2\,\mathrm{s}$, $L_\gamma = 1.6 \times 10^{44}\,\mathrm{erg\,s^{-1}}$ (see table 3.1).

Since $W_{\max} > 10^{20}\,\mathrm{eV}$, NGC 1068 is capable of efficiently accelerating charged particles to UHE levels. In fact; isotropic UHECR is as high as $\sim 30\,\mathrm{UHECRs/100\,km^2\,/yr}$ (Table 3.1),

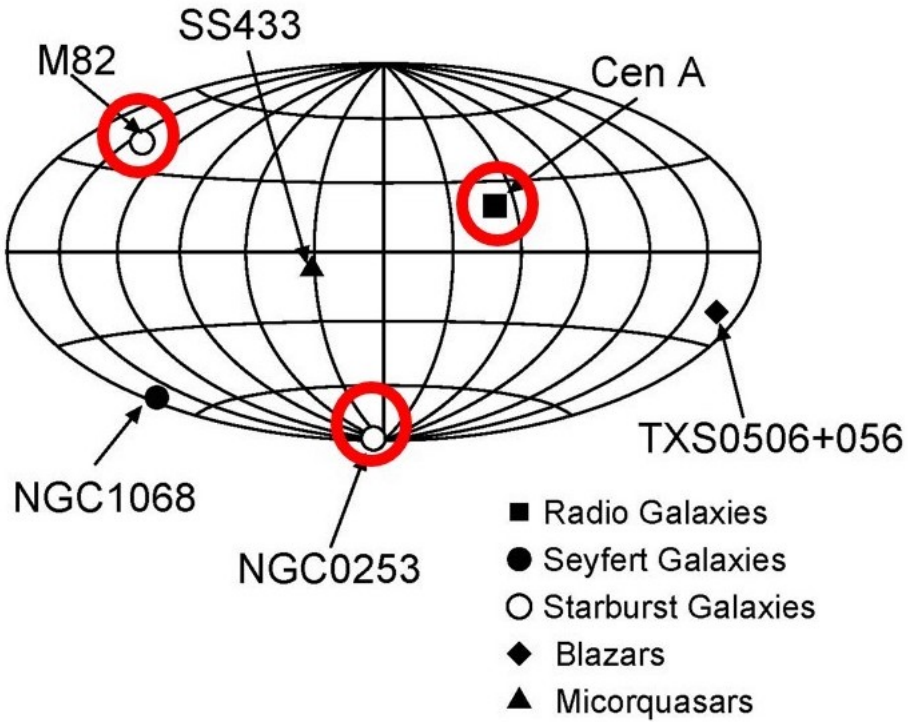


Figure 3.1: Prominent candidates of pin-pointed UHECR emission (from [67]). Based on morphology of the candidates and their existing data, WFA theory predicts M82, NGC0253, Cen A, and NGC4945 are promising UHECR sources. The three hot spots in the observed skymap (red circles) of UHECRs $> 6 \times 10^{19}$ eV [1] are consistent with prediction.

though the spot size would be too large (70 degree or more) due to intergalactic magnetic fields and a distance to Earth three times larger than M82, Cen A, and NGC 0253 [56].

There is no significant luminosity change in the intrinsic luminosity from the accretion disk of the nucleus of NGC 1068. Although Zaino *et al.* reported a time variability on the scale of 1-6 months [144], the detailed spectral analysis revealed that the variability is not due to the change in the intrinsic accretion rate but due to the change in the obscuring Compton thick cloud ($N_H > 10^{25}\,\mathrm{cm}^{-2}$) [93], which surrounds the nucleus. This view is consistent with the infrared and optical observations [138, 66].

Measurements from the *Fermi*-LAT telescope showed isotropic gamma-ray luminosity of $1.5 \times 10^{41}\,\mathrm{erg\,s}^{-1}$ [15]. This is inconsistent with the model prediction above (see Table 3.1). On the other hand, The MAGIC Telescopes' more recent results set an upper limit of gamma-ray flux above 200 GeV at $5.1 \times 10^{-13}\,\mathrm{erg\,cm}^{-2}\,\mathrm{s}^{-1}$ [13], which corresponds to an isotropic luminosity of $3.5 \times 10^{45}\,\mathrm{erg\,s}^{-1}$ that is slightly more than one order of magnitude larger when compared with the theoretical prediction.

The IceCube collaboration reported the positive detection of neutrinos at 1 TeV of $3 \times 10^{-13}\,\mathrm{TeV}^{-1}\,\mathrm{cm}^{-2}\,\mathrm{s}^{-1}$ from NGC 1068 [2]. Substituting $m = 1.6 \times 10^6$, $L_{\mathrm{rad}} = 1.8 \times 10^{45}\,\mathrm{erg\,s}^{-1}$, $\Omega = 4\pi$, and $\alpha = 0.1$ into equation 2.9, we obtain the theoretical isotropic flux as: $2.2 \times 10^{-11}\,\mathrm{TeV}^{-1}\,\mathrm{cm}^{-2}\,\mathrm{s}^{-1}$. In other words, WFA theory can explain IceCube observation, if 1% of the neutrinos emitted from the jets travel towards Earth; the neutrinos from the jets are most likely to be strongly beamed.

It is possible there are two primary sources of neutrinos emitted from an AGN: magnetic reconnection in the accretion disk, and WFA in the jets. Khiali *et al.* showed that magnetic reconnection in the disk can account for neutrino emission below 10 PeV in BL Lacs and low-luminosity AGNs [76]. Rodreiguez-Ramirez *et al.* did the same for Cen A, the nearest AGN whose jets happen to be nearly perpendicular to our LOS providing good resolution

of the galactic center [122]. WFA is capable of creating neutrinos well beyond 10 PeV by accelerating protons to ZeV energies and beyond, which then collide with slower protons. Our estimate for the neutrino flux at 100 TeV for blazar TXS 0506+056 is within 50%, but our estimate for NGC 1068, whose jets are not aligned with our LOS, at 1 TeV was roughly 2 orders of magnitude larger. Therefore, it may be the case that WFA can only explain axially emitted neutrinos, produced in the jet, far away from the central object. Future observations of neutrino emissions from blazars could confirm this.

3.4 Starburst Galaxy: M82

M82 is a starburst galaxy at a distance of 3.6 Mpc from Earth [52] in the constellation Ursa Major. The starburst activity takes place in a relatively small central region, radius of ~ 200 pc [143] from the dynamic center of the galaxy.

Ultra luminous X-ray (ULX) sources of luminosity $\gtrsim 10^{40}\,\mathrm{erg\,s^{-1}}$ inside M82 has been observed (see [72] & the references therein). Among them, M82 X-1 is the brightest ULX in M82, located about 200 pc away from the dynamic center of the galaxy [90, 139, 114, 42, 51]. There has been a lot of discussions in the past 20 years regarding the mass of M82 X-1, which has converged to the intermediate mass range, in other words $10^2 - 10^3\ M_\odot$. We adopt the mass of $400\,M_\odot$ by [113], who used QPO frequency to fit a mass value. Substituting $m = 4 \times 10^2$ and $L_{\mathrm{rad}} = 2 \times 10^{41}\,\mathrm{erg\,s^{-1}}$, and $\alpha = 0.1$ into equations 2.4, 2.1, 2.2, and 2.7, we computed $W_{\mathrm{max}} = 1.5 \times 10^{23}\,\mathrm{eV}$, $2\pi/\omega = 3.5 \times 10^{-1}\,\mathrm{s}$, $1/\nu = 9.1 \times 10^{-2}\,\mathrm{s}$, and $L_\gamma = 1.7 \times 10^{40}\,\mathrm{erg\,s^{-1}}$, as shown in Table 3.1.

The WFA theory predicts that M82 X-1 is capable of accelerating protons and nuclei to energies above 10^{20}eV, in spite of its less massive black hole ($\sim 400\,M_\odot$; Table 3.1). In fact; the Telescope Array (TA) team suggested that there is a hot spot in the northern sky of

arrival direction of the UHECRs above 57 EeV in close proximity to M82 [4] (see Fig. 3.1).

He *et al.* divided the events belonging to the northern hot spot into two by energy, and found that there was a systematic deviation between them [64]. Assuming that this is due to the deflection by the magnetic field [56], the position of the true source was estimated. While the estimated position, though extended to 10 degrees, included several high-energy celestial objects such as M82 and Mrk 180, only M82 was located within the GZK-horizon (100 Mpc), the limit UHECRs can travel without significant energy loss. The Telescope Array (TA) team detected 72 cosmic rays of 57 EeV in 5 years. Among them, 19 events are within the hot spot [4], while approximately 4.5 events were expected from uniform arrival. Since the effective area of TA is $700\,\mathrm{km}^2$, the observed excess flux in the hot spot direction is about $0.040\,\mathrm{UHECRs}/100\,\mathrm{km}^2/\mathrm{yr}$, which is in good agreement with the expected isotropic flux from equation 2.5 ($\sim 0.052\,\mathrm{UHECRs}/100\,\mathrm{km}^2/\mathrm{yr}$, as shown in Table 3.1).

The QPO period of M82 X-1 is observed in X-ray band to be 0.2 s [113]. As we have carried out in chapters 3.1 and 3.3, the theoretical recurrence time is $1/\nu = 9.23 \times 10^{-2}$ s (see table 3.1). This predicted value is consistent with the QPO period within a factor of two.

In the WFA theory, electrons can also be accelerated in a similar way that protons are (see Fig. 2.1B). This is separate from the electron cloud that is accelerated in front of the electromagnetic wave. The high energy electrons, accelerated in the wakefield in the direction of the jet, emit gamma rays by synchrotron radiation due to interaction with magnetic perturbations in the jets. As previously mentioned the gamma-ray luminosity of M82 X-1 is predicted to be $1.7 \times 10^{40}\,\mathrm{erg/s}$ (Table 3.1). On the other hand, a bright and isolated gamma-ray excess, consistent with the location of the position of M82 of 100 MeV to 700 GeV gamma-rays that are isotropic in luminosity of 1.5×10^{40} erg/s with *Fermi*-LAT [15]). This is consistent with the theoretical prediction, though it might just be chance, taking into account the anisotropic nature of WFA theory (particle trajectories are predominantly linear). We cannot observe M82 and its jets along their axis (like a blazar),

therefore observational data samples oblique emissions, which we have used in our model predictions. Although it is encouraging that our predictions are consistent with data, both heavily underreport the true total luminosity, and flux of each signal.

3.5 Starburst Galaxy: NGC 0253

NGC 0253 is a nearly edge-on starburst galaxy located 3.5 ± 0.2 Mpc from the Earth [118] in the constellation Sculptor. The Pierre Auger Collaboration reanalyzed the data of arrival direction observed by Pierre Auger Observatory (PAO) and found that a significant (4σ level) enhancement in the arrival direction map of UHECRs above 39 EeV with the search radius of 12.9 degree toward nearby starburst galaxies, NGC 0253 (Fig. 3.1) [1]. The result is consistent with the data of Telescope Array team, though statistically marginal [1, 24].

Gutiérrez *et al.* proposed two candidates for the source of UHECRs [60]: TH2 [141] and NGC253 X-1. Although TH2 was presumed the brightest radio source nearly coincident to the center of the galaxy, the recent observation by ALMA revealed that the position of TH2 exactly coincides to one of the knots in the central region of NGC 0253, which are most likely HII regions excited by young compact star clusters. The mass of the clusters are estimated as $10^6 M_\odot$ and are not likely to have any blackholes, since there are no X-ray emissions. Although one may still assume a hidden non-accreting black hole in the cluster, any blackhole without accretion cannot emit any energy. They assumed a strong magnetic field of 10^4 G around the blackhole to produce jet luminosity through the Blandford-Znajek effect [60, 32]. However, this magnetic field will decay rapidly if there is no matter accreting on the blackhole, and thus the luminosity in equation 3 of [60] is not sustainable. In conclusion, TH2 is unlikely to be a source of UHECRs.

Ultra Luminous X-ray Sources (ULXs), on the other hand, are promising as UHECR sources,

such as NGC 0253 X-1, if we take into account wakefield acceleration. NGC 0253 harbors at least three ULXs with the luminosity ranging between $(2.4-4.1)\times10^{39}\,\mathrm{erg\,s^{-1}}$ [26]. The sum of the luminosities of the ULXs reaches $9.1\times10^{39}\,\mathrm{erg\,s^{-1}}$ as shown in Table 3.1. They are considered to be intermediate black holes with masses that range from $10^2-10^4\,M_\odot$. In fact, we can estimate the mass to be $6.1\times10^2 M_\odot$ by substituting $\alpha=0.1$, $L_{\mathrm{rad}}=9.1\times10^{39}\,\mathrm{erg\,s^{-1}}$, and $\dot{m}=0.1$ into equation 1.4. Substituting $m=6.1\times10^2$ and $L_{\mathrm{rad}}=9.1\times10^{39}\,\mathrm{erg\,s^{-1}}$, and $\alpha=0.1$ into equations 2.4, 2.1, 2.2, and 2.7, we can derive $W_{\mathrm{max}}=1.8\times10^{21}\,\mathrm{eV}$, $2\pi/\omega=1.5\times10^{-2}\,\mathrm{s}$, $1/\nu=1.4\times10^{-1}\,\mathrm{s}$, and $L_\gamma=7.9\times10^{38}\,\mathrm{erg\,s^{-1}}$, as shown in Table 3.1.

The maximum energy of protons are estimated to be $W_{\mathrm{max}}=1.8\times10^{21}\,\mathrm{eV}$. The expected UHECR flux ($0.013\,\mathrm{UHECRs/100\,km^2/yr}$) is approximately a factor of 5 larger than the observed flux ($0.0026\,\mathrm{UHECRs/100\,km^2/yr}$) for the isotropic distribution, as seen in Table 3.1 within of a factor of five.

The episodic recurrence time is estimated by our WFA model to be $1/\nu=1.4\times10^{-1}\,\mathrm{s}$. [26] reports significant variabilities can be seen in 100 second bin, which are much longer when compared with the theoretical predictions. Since observations for very short time variabilities (less than seconds) have unfortunately not been done for the ULXSs in NGC 253, the theory is not constrained by the observations.

The theoretical gamma-ray luminosity is estimated to be $L_\gamma=7.9\times10^{38}\,\mathrm{erg\,s^{-1}}$. The observed gamma-ray luminosity (isotropic) is $6.0\times10^{39}\,\mathrm{erg\,s^{-1}}$ in 1-100 GeV [15], which is one order of magnitude higher than the expected gamma-ray flux. Direct comparison of L_γ luminosity with our model is difficult, however, due to other contributions from supernova remnants [48].

3.6 Microquasar: SS 433

SS 433 is a galactic binary system consisting of a supergiant star $M = 10 - 30M_{\odot}$ and a compact object of $M = 2{-}3M_{\odot}$ (commonly considered to be a black hole) in the constellation Aquarius. The distance to the SS 433 system was estimated to be 3.5 kpc [33] and is located inside of the supernova remnant W50, which exploded 17-24 thousands years ago [57]. SS433 jet's have an approximate length of 40 pc, and a bulk velocity of $0.26c$ [88, 50]. The two precessing jets model is well established [49, 97, 9, 75, 65].

Kubota *et al.* determined the mass of the compact object from orbital analyses to be 2.5 $M_{\odot}$ [79]. According to [10, 37], the jet luminosity is as high as $10^{40}\,\mathrm{erg\,s^{-1}}$, because of super-critical accretion, in spite of very low luminosity ($10^{35-36}\,\mathrm{erg\,s^{-1}}$) in the X-ray band [125]. Substituting $m = 2.5$, $L_{\mathrm{rad}} = 1.0 \times 10^{40}\,\mathrm{erg\,s^{-1}}$, and $\alpha = 0.1$ into equations 2.4, 2.1, 2.2, and 2.7, we derived $W_{\max} = 8.1 \times 10^{22}\,\mathrm{eV}$, $2\pi/\omega = 1.7 \times 10^{-2}\,\mathrm{s}$, $1/\nu = 5.8 \times 10^{-4}\,\mathrm{s}$, and $L_{\gamma} = 8.7 \times 10^{38}\,\mathrm{ergs^{-1}}$, as shown in Table 3.1.

According to our WFA model, SS433 is capable of accelerating protons, and thus a potential source for UHECRs; in fact, the maximum acceleration energy $W_{\max}$ is as high as $3.5{\times}10^{21}\,\mathrm{eV}$ (Table 3.1). The UHECRs produced in SS433, may not be very localized unfortunately, since it is located near the galactic center, where the magnetic field is large compared with the outer region. It may produce a broad (more than several ten degrees) concentration toward the galactic center, together with other microquasars in the galactic center region [136].

Although a significant variation in flux at the time scale of 10 s was observed [119], there is no information in the millisecond range. Therefore, our prediction for the recurrence time, $1/\nu = 5.8 \times 10^{-4}$, is unconstrained by observation.

The model-predicted gamma-ray luminosity is $L_{\gamma} = 8.7 \times 10^{38}$ erg s^{-1} (Table 3.1). Since gamma rays are strongly beamed in the direction of the jets, they are not necessarily seen

from Earth; our LOS is not aligned with the jets of SS433. The angle between our LOS and the axis of the jet precession is about 74 degrees [38] and the precession angle is about 20 degrees [37]. Careful analysis of data from the Fermi gamma-ray observatory Large Area Telescope reveals that the SS433 system emits gamma rays with a peak around 250 MeV. It showed a modulation of $\sim 10^{-10}\,\mathrm{erg\,cm^{-2}\,s^{-1}}$ correlation with the precession period [117]. The corresponding isotropic luminosity is $3.6 \times 10^{37}\,\mathrm{erg\,s^{-1}}$. This component may be related to the gamma rays emitted from the electrons accelerated by wakefield in the jets, as suggested by Tajima *et al.* [136], though the observed flux is much less compared with the theoretical prediction for the case of isotropic emission, again likely due to the oblique angle between our LOS and the jet axis.

At 20 TeV, the HAWC detector reported the emission is spatially localized in the three lobes (e1, e2, and w1), 40 pc away from the SS433 system [10]. Since the lobes are located where the jets interact with the nebula gas, the gamma-rays are expected to be primarily a result of synchrotron emission from high energy electrons accelerated by the bow-shock which then collide with a magnetic field of $\sim 10\,\mu$Gauss produced by the interaction of jets with nebula clouds.

Galactic black hole binaries, such as SS433, Cyg X-1, Cyg X-3, Sco X-1 exhibit relativistic jets, violent variabilities in time scales ranging from milliseconds to years, and emit radiation from radio to very high energy gamma-rays ($\sim$ TeV). Because of such non-thermal phenomena, they are considered counterparts of quasars ($\sim 10^{6-9} M_\odot$) in million times smaller scales with masses of $\sim 10 M_\odot$ (i.e. micorquasars) yet they are capable of generating high energy gamma rays and UHECRs.

Chapter 4

Conclusions

4.1 Applications

The magnetic field structure of the jet, and the nature of plasma acceleration in the high-density region of the jet (nearest to the accretion) are relevant to other areas of study in plasma physics, such as high-density LWFA (Laser Wakefield Acceleration) and fusion in FRCs (Field Reversed Configuration). The seed-wave that creates the wakefield behind it is created when a large amount of matter from the accretion disk suddenly falls onto the central accreting engine (e.g. SMBH or neutron star) when, for example, a magneto-rotational instability occurs. This accretion creates an intense perturbation of the magnetic fields of the jet at their base (near the accretion disk). The perturbation of the helical magnetic field of the jet occurs in the over-dense ($n_e > n_c$ where n_c is the critical density of the wave and n_e is the electron density of the plasma) area of the jet, therefore the perturbation will propagate along the field lines as an Alfvén wave. As shown earlier, the Alfvén speed of the jet is nearly equal to the speed of light, and thus the phase velocity of the wave is fast enough that bulk-plasma interaction will not occur, but instead wakefield acceleration can.

Magnetic WFA is largely unexplored, however, it could be useful in laboratory LWFA experiments in the case where low frequency waves are unable to penetrate a target medium because the electron density is too high. If a magnetic field were applied, low-frequency Alfvén waves could propagate through an otherwise over-dense medium. This is the case in WFA in AGN jets, where the plasma density is initially too high for the frequency of the wave to exist as a typical EM wave, but instead as an Alfvén wave. The wave eventually mode-converts into a regular EM wave. This is the nature-suggested natural transformation from $n_e > n_{cr}$ to $n_e < n_{cr}$ for LWFA. If the wave is intense enough to strip electrons from a high-density medium and propel them into a low-density region (such in the case of stripping electrons from carbon-nanotubes [105, 27]), then they can be accelerated via wakefiled in the lower density region where the wave's phase velocity, the Alfvén speed v_A, is much greater. then LWFA could in-principle accelerate high-energy charged particles from over-dense mediums. Thus we learn from nature that the smooth transition from high-density to low-density mediums may happen in the neighborhood of the critical density region in the lab.

The Keplerian motion of the accretion disk spawns helical jets by laterally twisting polar-oriented magnetic field lines. The MRI in the disk creates an extremely intense perturbation of the jet magnetic field, which then propagates as a shear, Alfvén ion-cyclotron (AIC) wave that travels outward from the core, along the jet. This AIC wave then eventually mode-converts into a typical electromagnetic wave was reaching the underdense region of the jet plasms, and excites a wakefield, which accelerates plasma in the jet parallel to its wave vector. The natural helical structure of the jet, and coherent acceleration of plasma along the narrow jet suggests this is a favorable structure for the confinement and transfer of plasma. Therefore, we propose a helical magnetic field may be beneficial to fusion devices, such as in Field-Reversed Configuration (FRC) type reactors, for increasing confinement. Also, if an AIC wave were applied to the end-plug of an FRC fusion device, such that it is resonant with the local cyclotron frequency, angular (perpendicular) momentum would be

absorbed by the species that is resonant with the wave, effectively decreasing the pitch-angle in velocity-space – preventing ions from escaping the mirror field. Confinement of the plasma would be improved while also heating the plasma [104, 87]. This inspires us that the nature producing accretion disk-triggered shear motion on the magnetic field can produce inward plasma flows, potentially reproducible in a magnetic confinement devices such as an FRC.

In 2000, well before the famous gravitational wave detection's by LIGO [5], Takahashi correctly predicted a burst of gamma-ray emission would coincide with neutron star-neutron star collisions [137]. LIGO and Fermi observed gravitational wave and nearly simultaneous (delayed only by 1.74s) arrival of a gamma-ray burst. Takahashi explained that the upon the merger of the two neutron stars, when all of the mass of the smaller neutron star is sucked into the central balck hole, an extremely intense bow-wake wave is created in the neutrino-cooled accetion disk (or neutrino-dominated accretion flows, NDAF), capable of exciting wakefields 6-7 orders of magnitude higher than radiation-cooled accretion disks (see figure 4.1).

4.2 Wakefield Acceleration in AGN Jets

The objects that we have detailed above, in reality, are only a few "good candidates" out of tens and maybe even thousands or more of blazars, quasars and microquasars that possess jets of parsec to hundreds of kiloparsec length and are capable of accelerating charged particles to energies $> 10^{26}$ eV (as shown in Table 3.1). WFA is almost certainly present in all astrophysical objects that have "jets," regardless if they are as small as a binary star (10-100 Ms) or as large as blazars ($\geq 10^8$ Ms); the parameter values change, but the physics is the same (or similar). Although we have primarily focused on extragalactic jets as candidates for WFA – resulting in pinpointed emission of UHECRs and correlated, localized emission of gamma-rays with pronounced structure – through chapters 3.1-3.5, we also find that jets

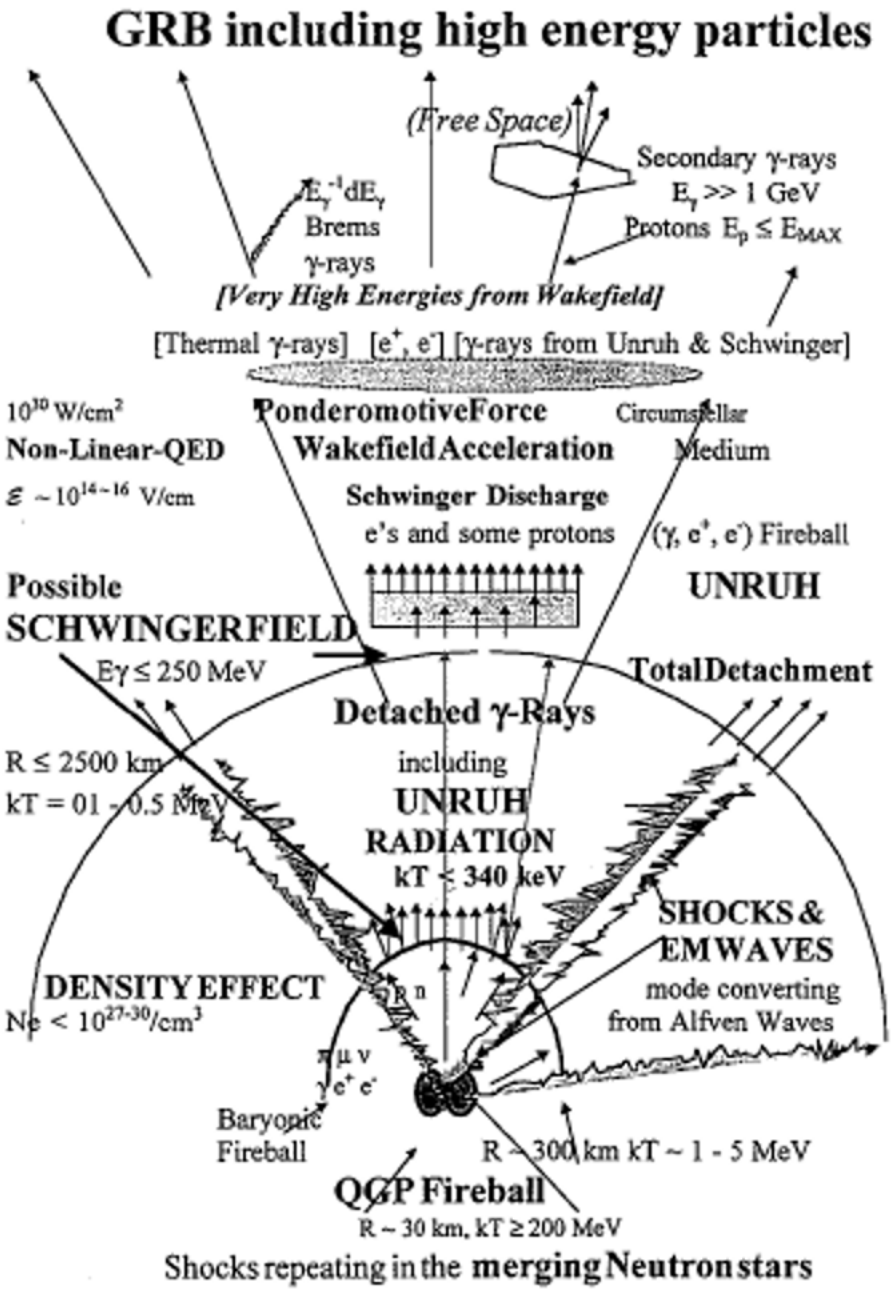


Figure 4.1: Upon the merger of two colliding neutron stars, gravitational waves are emitted, followed by a long-duration gamma-ray burst. Takahashi predicted that this dense burst of gamma-rays creates an extremely intesne bow-wake capable of creating a substantial flux of extremely high-energy cosmic-rays with energies exceeding 10^{21} eV. (from [137]).

from much smaller objects, namely microquasars in our own galaxy, are also capable of emitting UHECRs (including neutrinos) and simultaneously gamma-rays (see chapter 3.6). In fact our theory anticipates that much more microquasars are potential sources of a variety of signals including UHECRs.

Tables 3.1 summarizes the measurables of the six astrophysical objects we surveyed in relation to their observed properties along with the theoretically derived values. More accurate predictions of the UHECR flux, and luminosity can be calculated if the GZK limited maximum energy is substituted for W_{max} in equation 2.6. However, this is a straightforward calculation, and so the reporting of unattenuated values was favored to illustrate the capability of WFA at generating extremely high-energy charged particles in astrophysical jets of all sizes. In chapter 2 we adopted reasonable values for several model parameters including, but not limited to, $p,\ \kappa_T,\ \alpha$ since it is beyond the scope of this thesis to determine accurate values for each and every model parameter on a per source basis. We expect that the model predictions would be closer to their observational counterparts if more accurate values were used in the calculations. Despite some inaccuracy in the model parameters, WFA theory implies that the flux of all emitted particles and photons will be greatest when the observers LOS is parallel to the jet axis, such as the case for blazars, but closer to Earth than blazars typically are. This is because wakefields travel parallel to the jet and thus trapped charged particles accelerated by the wake also travel, and are eventually emitted parallel to the jet assuming little or no deflection from extrinsic factors. It is reasonable then to assume that the flux of these signals has a radial dependence on the distance from the jet axis that decreases outward. This may explain why we have only observed neutrinos from blazars, and not quasars. Furthermore, the most energetic particles are more likely to be emitted parallel or very near parallel to the jet axis since they are least susceptible to being perturbed. The anisotropy in emission of course also implies that the amount of observable UHECRs, gamma-rays, et cetera produced by nearby quasars and microquasars is less than it otherwise would be if their jets were oriented (anti)parallel to our LOS. Thus, it is expected that our

model predictions would over estimate observational data.

Our theory and predictions suggest that WFA is very capable of generating cosmic rays with energies equal to and even greater than the most energetic UHECRs that have ever been detected, as well as UHE gamma-rays and neutrinos. Many quasars, and microquasars alike show evidence of being pinpointed origins of UHE gamma-rays and UHECRs (and sometimes neutrinos) including the six objects studied herein. We acknowledge, however, that shock acceleration and magnetic reconnection are also potential sources for lower energy signals such as cosmic-rays below 10^{18} eV (before synchrotron radiation becomes insurmountable at large gamma factors), and most of the synchrotron emissions of VHE gamma-rays down to radio frequencies. In particular, magnetic reconnection may be capable of generating UHECRs as well.

A linear acceleration mechanism, such as WFA, is not hindered by deleterious synchrotron emissions. Furthermore, in the special case of blazars, our theory can explain time signatures, specifically anti-correlations in the spectral index and flux (Fig. 7 in [34]) observed in blazar 3C 453.4 that steady state theories, such as Fermi acceleration, cannot. Neutrino bursts, coincidental with gamma-ray bursts originating from blazars have recently been detected [54, 121]. This is also readily explained by WFA since it accelerates a dense cloud of electrons ahead of the wave that emit gamma-rays due to their orbit or collisions with magnetic inhomogenities, and pockets of UHE protons behind that can undergo collisions with slower protons to produce neutrinos, thereby creating simultaneous "bursts" of UHECRs, neutrinos, and gamma-rays. For decades astronomers have known that knots within AGN jets propagate at superluminal speeds, for example Cen A [70, 132]. This may be understood from WFA that it is natural to have extremely energetic, periodic structures that occur in the jets, part of which contain bow wakes [46, 47, 136] that form dense pockets of electrons propagating ahead of the pulse, and protons behind it.

WFA sheds new light on interesting time evolving processes, such as fluctuations in the

spectra of blazars, and the movement, and acceleration of matter inside astrophysical jets, and now even neutrino bursts. WFA coupled with the magneto-rotational instability (MRI) may be able to provide a virtually complete picture of the generation of UHECRs, UHE gamma rays, and dynamical time signature bursts and fluctuations from start to finish; beginning with MRI causing disk eruption and massive accretion of matter, and ending with the extremely fast particles colliding with decelerated particles in gaseous lobes at the end of the jets (to produce secondary particles and gamma-rays), or in Earth's atmosphere as UHECRs.

It was previously stated in chapter 1 that the condition for stable, bulk plasma acceleration via wakefields is satisfied since $v_{tr} \sim v_{ph} \gg v_{th}$. This does not imply that the entire plasma in the vicinty of the wakefield is trapped and accelerated for the duration of the wave. Instead, slower particles are accelerated for a lesser amount of time and even slower particles will experience multiple kicks as they randomly pass through accelerating-decelerating phases of the wake when the wave contains multiple frequencies. Chen *et al.* showed that the stochasticty of the kicks generates a power-law dependence of the particle energy spectrum with an index equal to 2 [36]. Lau *et al.* simulated relativistic wakefield acceleration using a 1D PIC code and plotted the resulting energy spectrum of the plasma in Fig. 7 of their paper [81]. It should be noted that the spectral index from WFA [98, 36] is similar to that of shock acceleration, however, the index can become greater than 2 in the case of WFA, see for example Fig. 4 in Canac *et al.* [34]. This is important for explaining the anti-correlations in flux and spectral-index of blazars.

Lower energy phenomena of these objects such as localized emissions of radio waves, soft x-rays with high intensities may be attributable to the disturbances arising not from the jets, but from the accretion disk itself. This may be a result of the MRI (not as well-organized as wakefield acceleration in the jets) that arises from the accretion disk itself. This is briefly explained in Fig. 1.4 (also see [63, 107, 131, 100, 85]). The time correlations (or lack of them)

in this lower energy range of emissions, along with high energy gamma rays and UHECRs (or neutrinos) may provide the subtle relation between the halo dynamics, exterior disk and interior disk, and jets. In appendix A a variation introduced by the spread of the jet, which changes theoretical values in Table 3.1 is explored.

The magnetic energy stored in an accretion disk obeys a power-law dependency on the BH mass [126]. This energy is the source from which both disk-jet magnetic reconnection and MRI [25, 46] draw their power from. That is why Fig. 2 in Singh *et al.*, and multiple figures in Kadowaki *et al.* show plots very similar to Fig. 2.3 [130, 74].

Further verification of wakefield acceleration theory in the universe conducted via multi-messenger observations including TeV gamma-ray telescope facilities is strongly encouraged, such as the Cerenkov Telescope Array (CTA; [16]), gravitational wave detectors like Advanced LIGO [3], the VIRGO [12], and KAGRA [18], and ultra high energy cosmic rays/neutrino observatories, such as Probe of Extreme Multi-Messenger Astrophysics, (POEMMA; [21]), and The Giant Radio Array for Neutrino Detection (GRAND; [19]). It is the wish of the author that WFA theory and the work presented here can contribute to these observational efforts.

Bibliography

[1] A. Aab et al. An indication of anisotropy in arrival directions of ultra-high-energy cosmic rays through comparison to the flux pattern of extragalactic gamma-ray sources. *The Astrophysical Journal Letters*, 853(2):L29, feb 2018.

[2] M. G. Aartsen et al. Time-integrated neutrino source searches with 10 years of icecube data. *Phys. Rev. Lett.*, 124:051103, Feb 2020.

[3] J. Aasi et al. Advanced LIGO. *Classical and Quantum Gravity*, 32(7):074001, mar 2015.

[4] R. U. Abbasi et al. Indications of Intermediate-scale Anisotropy of Cosmic Rays with Energy Greater Than 57 EeV in the Northern Sky Measured with the Surface Detector of the Telescope Array Experiment. *ApJ Letters*, 790(2):L21, Aug. 2014.

[5] B. P. Abbott et al. Gravitational Waves and Gamma-Rays from a Binary Neutron Star Merger: GW170817 and GRB 170817A. *ASTROPHYSICAL JOURNAL LETTERS*, 848(2), OCT 20 2017.

[6] B. P. Abbott et al. Multi-messenger Observations of a Binary Neutron Star Merger. *ASTROPHYSICAL JOURNAL LETTERS*, 848(2), OCT 20 2017.

[7] A. A. Abdo et al. DETECTION OF GAMMA-RAY EMISSION FROM THE STARBURST GALAXIES M82 AND NGC 253 WITH THE LARGE AREA TELESCOPE ON FERMI. *ASTROPHYSICAL JOURNAL LETTERS*, 709(2):L152, FEB 1 2010.

[8] A. A. Abdo et al. The First Catalog of Active Galactic Nuclei Detected by the Fermi Large Area Telescope. *ApJ*, 715(1):429–457, May 2010.

[9] G. O. Abell and B. Margon. A kinematic model for SS433. , 279(5715):701–703, June 1979.

[10] A. U. Abeysekara et al. Very-high-energy particle acceleration powered by the jets of the microquasar ss 433. *Nature*, 562(7725):82–85, 2018.

[11] J. Abraham et al. Correlation of the highest-energy cosmic rays with the positions of nearby active galactic nuclei. *Astroparticle Physics*, 29(3):188–204, 2008.

[12] T. Accadia et al. Status of the Virgo project. *CLASSICAL AND QUANTUM GRAVITY*, 28(11), JUN 7 2011.

[13] V. A. Acciari et al. Constraints on Gamma-Ray and Neutrino Emission from NGC 1068 with the MAGIC Telescopes. *ApJ*, 883(2):135, Oct. 2019.

[14] M. Ackermann et al. THE SECOND CATALOG OF ACTIVE GALACTIC NUCLEI DETECTED BY THE FERMI LARGE AREA TELESCOPE. *ApJ*, 743(2), DEC 20 2011.

[15] M. Ackermann et al. GeV Observations of Star-forming Galaxies with the Fermi Large Area Telescope. *ApJ*, 755(2):164, Aug. 2012.

[16] M. Actis et al. Design concepts for the Cherenkov Telescope Array CTA: an advanced facility for ground-based high-energy gamma-ray astronomy. *EXPERIMENTAL ASTRONOMY*, 32(3):193, DEC 2011.

[17] F. Aharonian et al. Discovery of Very High Energy γ-Ray Emission from Centaurus a with H.E.S.S. *ApJ Letters*, 695(1):L40–L44, Apr. 2009.

[18] T. Akutsu et al. Construction of KAGRA: an underground gravitational-wave observatory. *Progress of Theoretical and Experimental Physics*, 2018(1), 01 2018. 013F01.

[19] J. Alvarez-Muniz et al. The Giant Radio Array for Neutrino Detection (GRAND): Science and design. *SCIENCE CHINA-PHYSICS MECHANICS & ASTRONOMY*, 63(1), AUG 4 2019.

[20] H. Alvén. *Cosmic Plasma*. Springer Dordrecht, 1981.

[21] L. A. Anchordoqui, D. R. Bergman, M. E. Bertaina, F. Fenu, J. F. Krizmanic, A. Liberatore, A. V. Olinto, M. H. Reno, F. Sarazin, K. Shinozaki, J. F. Soriano, R. Ulrich, M. Unger, T. M. Venters, and L. Wiencke. Performance and science reach of the Probe of Extreme Multimessenger Astrophysics for ultrahigh-energy particles. , 101(2), JAN 24 2020.

[22] S. Ansoldi, L. Antonelli, C. Arcaro, D. Baack, A. Babić, B. Banerjee, P. Bangale, U. B. de Almeida, et al. The Blazar TXS 0506+056 Associated with a High-energy Neutrino: Insights into Extragalactic Jets and Cosmic-Ray Acceleration. *ApJ Letters*, 863(1), 2018.

[23] K. Asada and M. Nakamura. The Structure of the M87 Jet: A Transition from Parabolic to Conical Streamlines. *ApJ Letters*, 745(2):L28, Feb 2012.

[24] R. Attallah and D. Bouchachi. Ultrahigh energy cosmic rays from nearby starburst galaxies. *Monthly Notices of the Royal Astronomical Society*, 478(1):800–806, 04 2018.

[25] S. Balbus and J. Hawley. *ApJ*, 376:214–222, 1991.

[26] R. Barnard. In-depth studies of the NGC 253 ULXs with XMM-Newton: remarkable variability in ULX1, and evidence for extended coronae. , 404:42, 2010.

[27] E. Barraza-Valdez, T. Tajima, D. Strickland, and D. E. Roa. Laser beat-wave acceleration near critical density. *Photonics*, 9(7), 2022.

[28] A. R. Bell. The acceleration of cosmic rays in shock fronts – I. *Monthly Notices of the Royal Astronomical Society*, 182(2):147–156, Feb. 1978. _eprint: https://academic.oup.com/mnras/article-pdf/182/2/147/3710138/mnras182-0147.pdf.

[29] R. Blandford and D. Eichler. Particle acceleration at astrophysical shocks: A theory of cosmic ray origin. *Physics Reports*, 154(1):1–75, 1987.

[30] R. D. Blandford. Accretion Disc Electrodynamics — A Model for Double Radio Sources. *Monthly Notices of the Royal Astronomical Society*, 176(3):465–481, Sept. 1976. _eprint: https://academic.oup.com/mnras/article-pdf/176/3/465/9332949/mnras176-0465.pdf.

[31] R. D. Blandford and D. G. Payne. Hydromagnetic flows from accretion discs and the production of radio jets. *Monthly Notices of the Royal Astronomical Society*, 199(4):883–903, Aug. 1982.

[32] R. D. Blandford and R. L. Znajek. Electromagnetic extraction of energy from Kerr black holes. , 179:433–456, May 1977.

[33] K. M. Blundell and M. G. Bowler. Symmetry in the Changing Jets of SS 433 and Its True Distance from Us. *ApJ Letters*, 616(2):L159–L162, Dec. 2004.

[34] N. E. Canac, K. N. Abazajian, T. Tajima, T. Ebisuzaki, and S. Horiuchi. Observational signatures of gamma-rays from bright blazars and wakefield theory. *Monthly Notices of the Royal Astronomical Society*, 493(2):2229–2237, 02 2020.

[35] K. Chatterjee, M. Liska, A. Tchekhovskoy, and S. B. Markoff. Accelerating AGN jets to parsec scales using general relativistic MHD simulations. *Monthly Notices of the Royal Astronomical Society*, 490(2):2200–2218, 09 2019.

[36] P. Chen, T. Tajima, and Y. Takahashi. Plasma Wakefield Acceleration for Ultrahigh-Energy Cosmic Rays. *Physical Review Letters*, 89(16):161101, Sept. 2002.

[37] Cherepashchuk, A. M., Sunyaev, R. A., Fabrika, S. N., Postnov, K. A., Molkov, S. V., Barsukova, E. A., Antokhina, E. A., Irsmambetova, T. R., Panchenko, I. E., Seifina, E. V., Shakura, N. I., Timokhin, A. N., Bikmaev, I. F., Sakhibullin, N. A., Aslan, Z., Khamitov, I., Pramsky, A. G., Sholukhova, O., Gnedin, Yu. N., Arkharov, A. A., and Larionov, V. M. Integral observations of ss433: Results of a coordinated campaign. *A&A*, 437(2):561–573, 2005.

[38] V. V. Davydov, V. F. Esipov, and A. M. Cherepashchuk. Spectroscopic monitoring of SS 433: A search for long-term variations of kinematic model parameters. *Astronomy Reports*, 52(6):487–506, June 2008.

[39] E. M. de Gouveia Dal Pino and G. Kowal. Particle Acceleration by Magnetic Reconnection. volume 407, pages 373–398. 2015. arXiv:1302.4374 [astro-ph].

[40] E. M. de Gouveia Dal Pino, G. Kowal, and A. Lazarian. Fermi acceleration in magnetic reconnection sites. volume 488 of *8th International Conference of Numerical Modeling of Space Plasma Flows (ASTRONUM 2013)*, page 8, 2013.

[41] E. M. de Gouveia Dal Pino and A. Lazarian. Production of the large scale superluminal ejections of the microquasar GRS 1915+105 by violent magnetic reconnection. *Astronomy & Astrophysics*, 441(3):845–853, Oct. 2005.

[42] G. C. Dewangan, L. Titarchuk, and R. E. Griffiths. Black Hole Mass of the Ultraluminous X-Ray Source M82 X-1. *ApJ Letters*, 637(1):L21–L24, Jan. 2006.

[43] T. DeYoung. The HAWC observatory. *NUCLEAR INSTRUMENTS & METHODS IN PHYSICS RESEARCH SECTION A-ACCELERATORS SPECTROMETERS DETECTORS AND ASSOCIATED EQUIPMENT*, 692:72, NOV 11 2012. 3rd Roma International Conference on Astroparticle Physics (RICAP), Roma Tre Univ, Rome, ITALY, MAY 24-27, 2011.

[44] A. di Matteo, T. Fujii, and K. Kawata. Investigating an angular correlation between nearby starburst galaxies and UHECRs with the Telescope Array experiment. In *European Physical Journal Web of Conferences*, volume 210 of *European Physical Journal Web of Conferences*, page 01007, Oct. 2019.

[45] A. Djannati-Atai. Status of very high energy gamma-ray Astronomy as of early 2008. *NUCLEAR INSTRUMENTS & METHODS IN PHYSICS RESEARCH SECTION A-ACCELERATORS SPECTROMETERS DETECTORS AND ASSOCIATED EQUIPMENT*, 602(1):28, APR 11 2009. 3rd International Workshop on a Very Large Volume Neutrino Telescope for the Mediterranean Sea, Toulon, FRANCE, APR 22-24, 2008.

[46] T. Ebisuzaki and T. Tajima. Astrophysical ZeV acceleration in the relativistic jet from an accreting supermassive blackhole. *ASTROPARTICLE PHYSICS*, 56:9, APR 2014.

[47] T. Ebisuzaki and T. Tajima. Pondermotive acceleration of charged particles along the relativistic jets of an accreting blackhole. *EUROPEAN PHYSICAL JOURNAL-SPECIAL TOPICS*, 223(6):1113, MAY 2014.

[48] B. Eichmann and J. B. Tjus. THE RADIO-GAMMA CORRELATION IN STARBURST GALAXIES. *ApJ*, 821(2), APR 20 2016.

[49] A. C. Fabian and M. J. Rees. SS 433: a double jet in action? , 187:13P–16, Apr. 1979.

[50] S. Fabrika. The jets and supercritical accretion disk in SS433. *Astrophys. Space Phys. Res.*, 12:1–152, Jan. 2004.

[51] H. Feng and P. Kaaret. IDENTIFICATION OF THE x-RAY THERMAL DOMINANT STATE IN AN ULTRALUMINOUS x-RAY SOURCE IN m82. *ApJ*, 712(2):L169–L173, mar 2010.

[52] W. L. Freedman, S. M. Hughes, B. F. Madore, J. R. Mould, M. G. Lee, P. Stetson, R. C. Kennicutt, A. Turner, L. Ferrarese, H. Ford, J. A. Graham, R. Hill, J. G. Hoessel, J. Huchra, and G. D. Illingworth. The Hubble Space Telescope Extragalactic Distance Scale Key Project. I. The Discovery of Cepheids and a New Distance to M81. *ApJ*, 427:628, June 1994.

[53] Y. Fukazawa, K. Hiragi, S. Yamazaki, M. Mizuno, K. Hayashi, K. Hayashi, S. Nishino, H. Takahashi, and M. Ohno. Suzaku View of X-Ray Spectral Variability of the Radio Galaxy Centaurus A: Partial Covering Absorber, Reflector, and Possible Jet Component. *ApJ*, 743(2):124, Dec. 2011.

[54] S. Garrappa et al. Investigation of two ifermi/i-LAT gamma-ray blazars coincident with high-energy neutrinos detected by IceCube. *The Astrophysical Journal*, 880(2):103, jul 2019.

[55] D. Gilden and T. Tajima. Magnetic field reconnection in differentially rotating accretion disks. In *Proc. IAU Symposium 107*, pages 477–480, Aug 1985.

[56] N. Globus, D. Allard, and E. Parizot. Propagation of high-energy cosmic rays in extragalactic turbulent magnetic fields: resulting energy spectrum and composition. , 479(1):97, FEB 2008.

[57] P. T. Goodall, F. Alouani-Bibi, and K. M. Blundell. When microquasar jets and supernova collide: hydrodynamically simulating the SS 433-W 50 interaction. , 414(4):2838–2859, July 2011.

[58] A. D. Goulding, D. M. Alexander, B. D. Lehmer, and J. R. Mullaney. Towards a complete census of active galactic nuclei in nearby galaxies: the incidence of growing black holes. , 406(1):597–611, July 2010.

[59] K. Greisen. END TO COSMIC-RAY SPECTRUM. , 16(17):748, 1966.

[60] E. M. Gutiérrez, G. E. Romero, and F. L. Vieyro. Cosmic rays from the nearby starburst galaxy NGC 253: the effect of a low-luminosity active galactic nucleus. *Monthly Notices of the Royal Astronomical Society*, 494(2):2109–2116, 03 2020.

[61] H. E. S. S. Collaboration. The γ-ray spectrum of the core of Centaurus A as observed with H.E.S.S. and Fermi-LAT. , 619:A71, Nov. 2018.

[62] J. P. Halpern, M. Eracleous, and J. R. Mattox. Redshifts of Candidate Gamma-Ray Blazars. , 125(2):572–579, Feb. 2003.

[63] C. Haswell, T. Tajima, and J.-I. Sakai. *ApJ*, 401:495, 1992.

[64] H.-N. He, A. Kusenko, S. Nagataki, B.-B. Zhang, R.-Z. Yang, and Y.-Z. Fan. Monte Carlo Bayesian search for the plausible source of the Telescope Array hotspot. , 93(4):043011, Feb. 2016.

[65] R. M. Hjellming and K. J. Johnston. An analysis of the proper motions of SS 433 radio jets. *ApJ Letters*, 246:L141–L145, June 1981.

[66] Hönig, S. F. and Kishimoto, M. Constraining properties of dusty environments by infrared variability. *A&A*, 534:A121, 2011.

[67] G. B. Huxtable, N. Eltawil, W.-X. Feng, G. Player, W. Wang, T. Tajima, and T. Ebisuzaki. Signatures of wakefield acceleration in astrophysical jets via gamma-rays and UHECRs. *Monthly Notices of the Royal Astronomical Society*, 522(4):5402–5414, 05 2023.

[68] IceCube Collaboration et al. Multimessenger observations of a flaring blazar coincident with high-energy neutrino IceCube-170922A. *Science*, 361(6398):eaat1378, July 2018.

[69] IceCube Collaboration et al. Neutrino emission from the direction of the blazar TXS 0506+056 prior to the IceCube-170922A alert. *Science*, 361(6398):147–151, July 2018.

[70] F. P. Israel. Centaurus a –ngc 5128. *The Astronomy and Astrophysics Review*, 8(4):237–278, 1998.

[71] J. D. Jackson. *Classical Electrodynamics*. Wiley, 1975.

[72] X. jie Xu, J. Liu, and J. Liu. A LIKELY MICRO-QUASAR IN THE SHADOW OF m82 x-1. *The Astrophysical Journal*, 799(2):L28, jan 2015.

[73] E. Jourdain, L. Bassani, J. P. Roques, P. Mandrou, J. Ballet, A. Claret, P. Laurent, F. Lebrun, A. Finogenov, E. Churazov, M. Gilfanov, R. Sunyaev, A. Dyachkov, N. Khavenson, K. Sukhanov, and R. Kremnev. On the Hard X-Ray Variability of Centaurus A. *ApJ*, 412:586, Aug. 1993.

[74] L. H. S. Kadowaki, E. M. d. G. D. Pino, and C. B. Singh. THE ROLE OF FAST MAGNETIC RECONNECTION ON THE RADIO AND GAMMA-RAY EMISSION FROM THE NUCLEAR REGIONS OF MICROQUASARS AND LOW LUMINOSITY AGNs. *The Astrophysical Journal*, 802(2):113, Mar. 2015.

[75] J. I. Katz, S. F. Anderson, B. Margon, and S. A. Grandi. Nodding motions of accretion rings and disks : a short-term period inSS 433. *ApJ*, 260:780–793, Sept. 1982.

[76] B. Khiali and E. M. de Gouveia Dal Pino. Very high energy neutrino emission from the core of low luminosity AGNs triggered by magnetic reconnection acceleration. *Monthly Notices of the Royal Astronomical Society*, 455(1):838–845, Jan. 2016. arXiv:1506.01063 [astro-ph].

[77] M. Kole. Cosmic plasma-wakefield acceleration. *CERN Courier*, 61:11, Jan. 2021.

[78] K. Kotera and A. V. Olinto. The astrophysics of ultrahigh-energy cosmic rays. *Annual Review of Astronomy and Astrophysics*, 49(1):119–153, 2011.

[79] K. Kubota, Y. Ueda, N. Kawai, T. Kotani, M. Namiki, K. Kinugasa, S. Ozaki, T. Iijima, S. Fabrika, T. Yuasa, S. Yamada, and K. Makishima. Suzaku X-Ray and Optical Spectroscopic Observations of SS 433 in the 2006 April Multiwavelength Campaign. , 62:323, Apr. 2010.

[80] R. C. Lamb and D. J. Macomb. Point Sources of GeV Gamma Rays. *ApJ*, 488(2):872–880, Oct. 1997.

[81] C. Lau, P. Yeh, O. Luk, J. McClenaghan, T. Ebisuzaki, and T. Tajima. Ponderomotive acceleration by relativistic waves. *Physical Review Special Topics - Accelerators and Beams*, 18(2):024401, Feb. 2015.

[82] C. R. Lawrence, C. L. Bennett, J. A. Garcia-Barreto, P. E. Greenfield, and B. F. Burke. 5 GHz observations of sources in the Arecibo 611 MHz survey. *ApJ Supplement Series*, 51:67–114, Jan. 1983.

[83] J. N. Leboeuf, T. Tajima, C. F. Kennel, and J. M. Dawson. Global simulation of the time-dependent magnetosphere. , 5(7):609–612, July 1978.

[84] J. N. Leboeuf, T. Tajima, C. F. Kennel, and J. M. Dawson. Global simulations of the three-dimensional magnetosphere. , 8(3):257–260, Mar. 1981.

[85] T. Liu, W.-M. Gu, and B. Zhang. Neutrino-dominated accretion flows as the central engine of gamma-ray bursts. *New Astronomy Reviews*, 79:1–25, 2017.

[86] R. V. E. Lovelace. Dynamo model of double radio sources. *Nature*, 262(5570):649–652, 1976.

[87] R. M. Magee, A. Necas, R. Clary, S. Korepanov, S. Nicks, T. Roche, M. C. Thompson, M. W. Binderbauer, and T. Tajima. Direct observation of ion acceleration from a beam-driven wave in a magnetic fusion experiment. *Nature Physics*, 15(3):281–286, 2019.

[88] B. Margon, S. F. Anderson, L. H. Aller, R. A. Downes, and C. D. Keyes. Rapid intensity variability in the jets of SS 433. *ApJ*, 281:313–317, June 1984.

[89] E. Massaro, P. Giommi, C. Leto, P. Marchegiani, A. Maselli, M. Perri, S. Piranomonte, and S. Sclavi. Roma-BZCAT: a multifrequency catalogue of blazars. , 495(2):691–696, Feb. 2009.

[90] H. Matsumoto and T. G. Tsuru. X-Ray Evidence of an AGN in M82. , 51:321–331, June 1999.

[91] R. Matsumoto and T. Tajima. Magnetic Viscosity by Localized Shear Flow Instability in Magnetized Accretion Disks. *ApJ*, 445:767, June 1995.

[92] R. Matsumoto, Y. Uchida, S. Hirose, K. Shibata, M. R. Hayashi, A. Ferrari, G. Bodo, and C. Norman. Radio Jets and the Formation of Active Galaxies: Accretion Avalanches on the Torus by the Effect of a Large-Scale Magnetic Field. *ApJ*, 461:115, Apr. 1996.

[93] G. Matt, S. Bianchi, M. Guainazzi, and S. Molendi. The high energy emission line spectrum of NGC 1068. , 414:155–161, Jan. 2004.

[94] J. H. Matthews, A. R. Bell, and K. M. Blundell. Particle acceleration in astrophysical jets. *New Astronomy Reviews*, 89:101543, 2020.

[95] T. E. Medina-Torrejón, E. M. de Gouveia Dal Pino, L. H. S. Kadowaki, G. Kowal, C. B. Singh, and Y. Mizuno. Particle acceleration by relativistic magnetic reconnection driven by kink instability turbulence in poynting flux–dominated jets. *The Astrophysical Journal*, 908(2):193, feb 2021.

[96] P. F. Michelson, W. B. Atwood, and S. Ritz. Fermi Gamma-ray Space Telescope: high-energy results from the first year. *REPORTS ON PROGRESS IN PHYSICS*, 73(7), JUL 2010.

[97] M. Milgrom. On the interpretation of the large variations in the line positions in SS433. , 76(1):L3–L6, June 1979.

[98] K. Mima, W. Horton, T. Tajima, and A. Hasegawa. Powerlaw energy spectrum and orbital stochasticity. *AIP Conference Proceedings*, 230(1):27–39, 1991.

[99] K. Mima, T. Tajima, and J. N. Leboeuf. Magnetic field generation by the rayleigh-taylor instability. *Phys. Rev. Lett.*, 41:1715–1719, Dec 1978.

[100] S. Mineshige. Accretion disk instabilities. *Astrophysics and Space Science*, 210(1):83–103, 1993.

[101] C. Misner, K. Thorne, and J. Wheeler. *Gravitation*. W H Freeman & Co, San Francisco, 1973.

[102] A. Mizuta, T. Ebisuzaki, T. Tajima, and S. Nagataki. Production of intense episodic Alfvén pulses: GRMHD simulation of black hole accretion discs. , 479(2):2534–2546, 07 2018.

[103] N. Neumayer. The Supermassive Black Hole at the Heart of Centaurus A: Revealed by the Kinematics of Gas and Stars. , 27(4):449–456, Oct. 2010.

[104] B. Nicks, R. Magee, A. Necas, and T. Tajima. Beam-driven ion-cyclotron modes in the scrape-off layer of a field-reversed configuration. *Nuclear Fusion*, 61(1):016004, nov 2020.

[105] B. S. Nicks, E. Barraza-Valdez, S. Hakimi, K. Chesnut, G. DeGrandchamp, K. Gage, D. Housley, G. Huxtable, G. Lawler, D. Lin, P. Manwani, E. Nelson, G. Player, M. Seggebruch, J. Sweeney, J. Tanner, K. Thompson, and T. Tajima. High-density dynamics of laser wakefield acceleration from gas plasmas to nanotubes. *Photonics*, 8(6), 2021.

[106] K. Nishikawa, Y. Mizuno, J. L. Gómez, I. Duţan, J. Niemiec, O. Kobzar, N. MacDonald, A. Meli, M. Pohl, and K. Hirotani. Rapid particle acceleration due to recollimation shocks and turbulent magnetic fields in injected jets with helical magnetic fields. *Monthly Notices of the Royal Astronomical Society*, 493(2):2652–2658, Apr. 2020.

[107] T. Okuda, K. Ono, M. Tabata, and S. Mineshige. DISK OSCILLATION MODEL FOR QUASI-PERIODIC LIGHT VARIATIONS IN CATACLYSMIC VARIABLES. , 254(3):427, FEB 1 1992.

[108] T. O'Neil. Collisionless damping of nonlinear plasma oscillations. *The Physics of Fluids*, 8(12):2255–2262, 1965.

[109] S. O'Sullivan, B. Reville, and A. M. Taylor. Stochastic particle acceleration in the lobes of giant radio galaxies. , 400(1):248–257, Nov. 2009.

[110] P. Padovani, F. Oikonomou, M. Petropoulou, P. Giommi, and E. Resconi. TXS0506+056, the first cosmic neutrino source, is not a BL Lac. *Monthly Notices of the Royal Astronomical Society: Letters*, 484(1):L104–L108, 01 2019.

[111] S. Paiano, R. Falomo, A. Treves, and R. Scarpa. The Redshift of the BL Lac Object TXS 0506+056. *ApJ Letters*, 854(2):L32, Feb. 2018.

[112] S. Paiano, M. Landoni, R. Falomo, A. Treves, and R. Scarpa. Spectroscopy of 10 γ-Ray BL Lac Objects at High Redshift. *ApJ*, 844(2):120, Aug. 2017.

[113] D. R. Pasham, T. E. Strohmayer, and R. F. Mushotzky. A 400-solar-mass black hole in the galaxy M82. , 513(7516):74–76, Sept. 2014.

[114] A. Patruno, S. Portegies Zwart, J. Dewi, and C. Hopman. The ultraluminous X-ray source in M82: an intermediate-mass black hole with a giant companion. , 370(1):L6–L9, July 2006.

[115] A. B. Pushkarev, Y. Y. Kovalev, M. L. Lister, and T. Savolainen. MOJAVE - XIV. Shapes and opening angles of AGN jets. , 468(4):4992–5003, Jul 2017.

[116] K. Ragan. Some recent highlights from VERITAS. *NUCLEAR INSTRUMENTS & METHODS IN PHYSICS RESEARCH SECTION A-ACCELERATORS SPECTROMETERS DETECTORS AND ASSOCIATED EQUIPMENT*, 692:24, NOV 11 2012. 3rd Roma International Conference on Astroparticle Physics (RICAP), Roma Tre Univ, Rome, ITALY, MAY 24-27, 2011.

[117] K. Rasul, P. M. Chadwick, J. A. Graham, and A. M. Brown. Gamma-rays from SS433: evidence for periodicity. , 485(2):2970–2975, May 2019.

[118] R. Rekola, M. Richer, M. McCall, M. Valtonen, J. Kotilainen, and C. Flynn. Distance to NGC 253 based on the planetary nebula luminosity function. , 361(1):330, JUL 2005.

[119] M. Revnivtsev, S. Fabrika, P. Abolmasov, K. Postnov, I. Bikmaev, R. Burenin, M. Pavlinsky, R. Sunyaev, I. Khamitov, and N. Sakhibullin. Broad band variability of SS433: accretion disk at work? , 447(2):545–551, Feb. 2006.

[120] J. L. Richards, W. Max-Moerbeck, V. Pavlidou, O. G. King, T. J. Pearson, A. C. S. Readhead, R. Reeves, M. C. Shepherd, M. A. Stevenson, L. C. Weintraub, L. Fuhrmann, E. Angelakis, J. A. Zensus, S. E. Healey, R. W. Romani, M. S. Shaw, K. Grainge, M. Birkinshaw, K. Lancaster, D. M. Worrall, G. B. Taylor, G. Cotter, and R. Bustos. Blazars in the Fermi Era: The OVRO 40 m Telescope Monitoring Program. *ApJ Supplement Series*, 194(2):29, June 2011.

[121] X. Rodrigues, S. Garrappa, S. Gao, V. S. Paliya, A. Franckowiak, and W. Winter. Multiwavelength and neutrino emission from blazar PKS 1502 106. *The Astrophysical Journal*, 912(1):54, may 2021.

[122] J. C. Rodriguez-Ramirez, E. M. de Gouveia Dal Pino, and R. Alves Batista. Numerical models of neutrino and gamma-ray emission from magnetic reconnection in the core of radio-galaxies. In *Proceedings of International Conference on Black Holes as Cosmic Batteries: UHECRs and Multimessenger Astronomy — PoS(BHCB2018)*, volume 329, page 014. SISSA Medialab, May 2019.

[123] R. E. Rothschild, A. Markowitz, E. Rivers, S. Suchy, K. Pottschmidt, M. Kadler, C. Mueller, and J. Wilms. TWELVE AND A HALF YEARS OF OBSERVATIONS OF CENTAURUS A WITH THE ROSSI X-RAY TIMING EXPLORER. *ApJ*, 733(1), MAY 20 2011.

[124] G. B. Rybicki and A. P. Lightman. *Radiative processes in astrophysics*. 1979.

[125] S. Safi-Harb and H. Ögelman. ROSAT and ASCA Observations of W50 Associated with the Peculiar Source SS 433. *ApJ*, 483(2):868–881, July 1997.

[126] N. I. Shakura and R. A. Sunyaev. Black holes in binary systems. Observational appearance. , 24:337–355, Jan. 1973.

[127] K. Shibata and Y. Uchida. A magnetodynamic mechanism for the formation of astrophysical jets. I - Dynamical effects of the relaxation of nonlinear magnetic twists. , 37(1):31–46, Jan. 1985.

[128] K. Shibata and Y. Uchida. A magnetohydrodynamic mechanism for the formation of astrophysical jets. II. Dynamical processes in the accretion of magnetized mass in rotation. , 38(5):631–660, Jan. 1986.

[129] K. Shibata and Y. Uchida. Formation of astrophysical jets by a contracting magnetic accretion disk. *Astrophysics and Space Science*, 118(1):443–447, 1986.

[130] C. B. Singh, E. M. de Gouveia Dal Pino, and L. H. S. Kadowaki. ON THE ROLE OF FAST MAGNETIC RECONNECTION IN ACCRETING BLACK HOLE SOURCES. *The Astrophysical Journal*, 799(2):L20, Jan. 2015.

[131] A. Smith, C. Haswell, and R. Hynes. VW Hyi: optical spectroscopy and Doppler tomography. , 369(4):1537, JUL 11 2006.

[132] B. Snios, S. Wykes, P. E. J. Nulsen, R. P. Kraft, E. T. Meyer, M. Birkinshaw, D. M. Worrall, M. J. Hardcastle, E. Roediger, W. R. Forman, and C. Jones. Variability and proper motion of x-ray knots in the jet of centaurus a. *The Astrophysical Journal*, 871(2):248, feb 2019.

[133] T. Tajima. Laser acceleration and its future. *Proceedings of the Japan Academy, Series B*, 86(3):147–157, 2010.

[134] T. Tajima and J. M. Dawson. Laser electron accelerator. *Phys. Rev. Lett.*, 43:267–270, Jul 1979.

[135] T. Tajima and K. Shibata. *Plasma Astrophysics*. Cambridge, Mass. : Perseus ; Boulder, Colo. ; Oxford : Westview, 2002.

[136] T. Tajima, X. Q. Yan, and T. Ebisuzaki. Wakefield acceleration. *Reviews of Modern Plasma Physics*, 4(1):7, 2020.

[137] Y. Takahashi, L. W. Hillman, and T. Tajima. *Relativistic Lasers and High Energy Astrophysics*, pages 171–221. Springer US, 01 2000.

[138] O. G. Taranova and V. I. Shenavrin. Infrared variability of the nucleus of the seyfert galaxy ngc 1068 in 1998–2004. *Astronomy Letters*, 32(7):439–445, 2006.

[139] T. G. Tsuru, H. Matsumoto, T. Inui, S. Matsushita, R. Kawabe, T. Harashima, T. Maihara, and F. Iwamuro. M82 X-1 —The Hyper Luminous X-Ray Source—. *Progress of Theoretical Physics Supplement*, 155:59–66, Jan. 2004.

[140] R. B. Tully and J. R. Fisher. *Nearby Galaxies Catalogue*. Cambridge University press, 1988.

[141] J. L. Turner and P. T. P. Ho. THE 1 PARSEC RADIO CORE AND POSSIBLE NUCLEAR EJECTION IN NGC-253. *ApJ*, 299(2):L77, DEC 15 1985.

[142] Y. Uchida and K. Shibata. Magnetically buffered accretion to a young star and the formation of bipolar flows. , 36:105–118, Jan. 1984.

[143] H. J. Völk, F. A. Aharonian, and D. Breitschwerdt. The nonthermal energy content and gamma ray emission of starburst galaxies and clusters of galaxies. *Space Science Reviews*, 75(1):279–297, 1996.

[144] A. Zaino, S. Bianchi, A. Marinucci, G. Matt, F. E. Bauer, W. N. Brandt, P. Gandhi, M. Guainazzi, K. Iwasawa, S. Puccetti, C. Ricci, and D. J. Walton. Probing the circumnuclear absorbing medium of the buried AGN in NGC 1068 through NuSTAR observations. *Monthly Notices of the Royal Astronomical Society*, 492(3):3872–3884, 01 2020.

[145] G. Zatsepin and V. Kuzmin. UPPER LIMIT OF SPECTRUM OF COSMIC RAYS. *JETP LETTERS-USSR*, 4(3):78, 1966.

Appendix A

Model Dependence on Arbitrary Jet Spreading Index

As has been examined in previous chapters 3.1-3.6, in interpreting the individual astrophysical objects and phenomena only one model may serve as sufficient in understanding those astrophysical objects. While the general theory we described through the excitation of the disk disturbances, including shaking of the jets, and the subsequent wakefield generation and acceleration of particles along the jets have turned out to be quite generic and deep rooted physics common among these objects and their phenomena, despite its disparate scales and mass differences of the central objects. There are some important individualities that may matter in detailed manifestations of the objects and parameters. One example of such may be the jet's spreading angle. Jets may be strongly collimated by the spiraling surrounding magnetic fields. This may relax certain constraints on phenomena and parameters. In the following derivations, a jet spreading index is introduced by one model parameter of the power-law index that determines the jet diameter as a function of the distance from the central object, as the jet particles and magnetic fields emanate outward.

The dependence of model parameters in the jet on distance from the bottom and how the waves propagate through it are assessed. First, assume that

$$b(D) = R_0 m((D/R_0 m)^p + 1) \tag{A1}$$

where $b(D)$ is the radius of the jet at distance D from the bottom of the jet, which, at the base, is assumed to be $b(0) = 3R_g = R_0 m$. Note, the second term in $b(D)$ is subsequently dropped since $D \gg R_0 m$ for the distances we are generally concerned with. Although the power-law index, p, is observed to be close to ~ 0.5 for the case of M87, the closest active galactic nuclei [23], and many other AGN jets [115], it may fall in the range of 0 (a cylinder) to 1 (a linear cone) for other AGNs and microquasars.

The cyclotron frequency ω'_c in the jet corrected for relativistic effects is given by

$$\omega'_{\rm c} = \frac{eB_{\rm jet}}{m_{\rm e} c\gamma} \tag{A2}$$

On the other hand, the magnetic field $B_{\rm jet}$ in the jet can be calculated assuming that the magnetic field flux is conserved in the jet.

$$B_{\rm jet} = [B_{\rm disk}(r=1)](b/mR_0)^{-2} \tag{A3}$$

$$= [B_{\rm disk}(r=1)]\left(\frac{D}{mR_0}\right)^{-2p} \tag{A4}$$

$$= \left(\frac{32\pi c^2}{\sqrt{6}\kappa_{\rm T} R_0}\right)^{1/2} m^{-1/2}\left(\frac{D}{mR_0}\right)^{-2p} \tag{A5}$$

Next, assume

$$\gamma = a_0 \equiv \frac{eE_w}{m_e \omega c} \tag{A6}$$

within the jet, where $E_w = \sqrt{v_A/c}\ B_{disk}(r = 1)$ and ω are the initial magnitude of the electric field and frequency of the wave, respectively. a_0 can be calculated, assuming that the wave intensity in the jet is conserved, *i.e.*, the flux $\Phi_{\rm w,jet}$ is inversely proportional to the cross-sectional area, πb^2, of the jet, such that

$$a_0(D) = a_0(D = R_0)\left(\frac{b(D)}{R_0 m}\right)^{-1}. \tag{A7}$$

In addition, Fig. 2.1 shows the ratio ω_c'/ω of the cyclotron frequency to the wave frequency and that of plasma frequency ω_p'/ω, plotted against the distance $D/(R_0 m)$ from the bottom of the jet for the typical cases ($\Gamma = 10$, $\alpha = 0.1$, $\xi = 10^{-2}$, $\dot{m} = 0.1$, and $m = 1, 10^4, 10^8$). Evaluating Eqn. A6, one gets

$$a_0(D) = \frac{\rm e}{m_{\rm e} c}\left(\frac{\sqrt{6}R_0}{3\pi\epsilon^3\kappa_{\rm T}}\right)^{1/2} \alpha^{3/4}\dot{m}^{3/2} m^{1/2}\left(\frac{D}{R_0 m}\right)^{-p} \tag{A8}$$

Substituting equations A5, and A6 into equation A2,

$$\omega_{\rm c}' = \frac{4\pi c\epsilon^{3/2}}{R_0}\frac{1}{\alpha^{3/4}\dot{m}^{3/2} m}\left(\frac{D}{R_0 m}\right)^{-p} \tag{A9}$$

On the other hand, the plasma frequency $\omega_{\rm p}'$ corrected for relativistic effects is given by

$$\omega_{\rm p}' = \left(\frac{4\pi n_{\rm jet} e^2}{m_{\rm e}\gamma}\right)^{1/2} \tag{A10}$$

The plasma density $n_{\rm jet}$ in the jet can be solved for as follows, if the kinetic luminosity of the jet is assumed to be:

$$L_{\rm jet} = n_{\rm jet}\mu m_{\rm H} c^3 \Gamma^2 \pi b^2 = \xi L_{\rm rad} \tag{A11}$$

is conserved through the jet.

$$n_{\rm jet} = \frac{2}{3\mu m_{\rm H}\kappa_{\rm T} R_0}\frac{\xi\dot{m}}{\Gamma^2 m}\left(\frac{D}{R_0 m}\right)^{-2p} \tag{A12}$$

Here, ξ is the ratio of the kinetic luminosity of the jet to the radiation luminosity, Γ is the bulk Lorentz factor, and $\mu = 1.29$ is the mean molecular weight of the accreting gas. Substituting equations A8 and A12 into equation A10, gives:

$$\omega'_{\rm p} = 2\left(\frac{2}{3}\right)^{3/8}\left(\frac{\pi^3 e^2 c^2 \epsilon^3}{\mu^2 m_H^2 \kappa_T R_0^3}\right)^{1/4}\frac{\xi^{1/2}}{\Gamma\alpha^{3/8}\dot{m}^{1/4}m^{3/4}}\left(\frac{D}{R_0 m}\right)^{-p/2} \tag{A13}$$

For most of the interesting cases, the relationship of $\omega'_{\rm c}$, $\omega'_{\rm p} > \omega$ holds; In other words, at the bottom of the jets, the plasma in the over dense state ($\omega'_{\rm p} > \omega$), where plasma waves and electromagnetic waves cannot propagate. On the other hand, Alfvénic waves can propagate, since $\omega'_{\rm c} > \omega$. The Alfvén velocity $V_{A,jet}$ at the bottom of the jet is given by

$$V_{\rm A,jet} = \frac{B_{\rm jet}}{\sqrt{4\pi m_{\rm H} n_{\rm jet}}} = 2\left(\frac{3}{2}\right)^{1/4}\frac{\mu^{1/2} c\Gamma}{\xi^{1/2}\dot{m}^{1/2}}\left(\frac{D}{R_0 m}\right)^{-p} \tag{A14}$$

In other words, the nominal values of the Alfvén velocity

$$V_{\rm A,jet} \sim 10^{13}\left(\frac{\Gamma}{10}\right)\left(\frac{\xi}{10^{-2}}\right)^{-1/2}\left(\frac{\dot{m}}{0.1}\right)^{-1/2}[{\rm cm\,s^{-1}}] \tag{A15}$$

This can approach the speed of light, when the approximation breaks down. Then the wave becomes that of EM waves in magnetized plasma. On the other hand, $\omega'_{\rm p} = \omega$ at the distance D_1 given by:

$$\left(\frac{D_1}{R_0 m}\right) = \left[\left(\frac{1}{27\sqrt{6}\pi}\right)\left(\frac{R_0 e^2}{\mu^2 m_{\rm H}^2 c^2 \kappa_T \epsilon}\right)\frac{\xi^2 \alpha^{1/2} \dot{m}^3 m}{\Gamma^4}\right]^{1/2p} \tag{A16}$$

Past the location of D_1 ($D > D_1$), $\omega > \omega'_{\rm p}$ so that the plasma wave (electromagnetic wave) is allowed to propagate. The electromagnetic waves propagated as Alfvén and whistler waves are converted into plasma waves (electromagnetic waves) by nonlinear mode-conversion when the wave frequency matches the plasma frequency. This $D > D_1$ leads to the bow wakefield acceleration as described in the next subsection.

The pondermotive force, $F_{\rm pm}$, which acts on the electrons caught in an intense electromagnetic wave is a force generated from the Lorentz force, $\left(\frac{v}{c}\right) \times B$, in the propagation direction of the electromagnetic wave. If the motion of the electrons by the wave is not relativistic ($a < 1$), it can be calculated as the force resulting from the average of the profiles of the electromagnetic pulses. In the relativistic regime ($a > 1$), this force is more simplified. Since the particle velocity asymptotically approaches the light velocity and if the plasma satisfies the under dense ($\omega > \omega'_p$) condition as well, then $B = E$. In this case, $F_{\rm pm}$, is given by

$$F_{\rm pm} = \Gamma m_{\rm e} e c a \omega \tag{A17}$$

Charged particles are accelerated by an electric field generated by bow wakefield (longitudinal polarization of electronic distributions). As shown in Fig. 2.1, protons are accelerated at the back slope of the wakefield, while electrons are accelerated at the front slope. The

acceleration force $F_{\rm acc}$ is given by

$$F_{\rm acc} = zF_{\rm pm} = z\Gamma eE_{\rm w}\left(\frac{D}{R_0}\right)^{-p} \tag{A18}$$

$$= \frac{ec}{3}\left(\frac{\pi}{\epsilon\kappa_{\rm T}R_0}\right)^{1/2}\frac{z\Gamma\alpha^{1/4}\dot{m}^{1/2}}{m^{1/2}}\left(\frac{D}{R_0 m}\right)^{-p} \tag{A19}$$

Here z is the charge of the particle. The maximum energy, $W_{\rm max}$, obtained by the particle is determined by integrating $F_{\rm acc}$ over the acceleration distance, D_3

$$W_{\rm max} = \int_0^{D_3} F_{\rm acc}dD \tag{A20}$$

$$= \frac{ec}{3}\left(\frac{\pi}{\epsilon\kappa_{\rm T}R_0}\right)^{1/2}\frac{z\Gamma\alpha^{1/4}\dot{m}^{1/2}}{m^{1/2}}\int_0^{D_3}\left(\frac{D}{R_0 m}\right)^{-p}dD \tag{A21}$$

$$= \frac{2ec}{3}\left(\frac{\pi R_0}{\epsilon\kappa_{\rm T}}\right)^{1/2} z\Gamma\alpha^{1/4}\dot{m}^{1/2}m^{1/2}\left(\frac{D_3}{R_0 m}\right)^{1-p}. \tag{A22}$$

Since generally $D_3 \gg D_1$ it suffices to integrate from along the range [0, D_3] for simplicity. The acceleration distance, D_3, is evaluated as:

$$D_3 = \frac{e}{432 m_{\rm e}c}\left(\frac{R_0^3}{\pi^3\epsilon^5\kappa_{\rm T}}\right)^{1/2}\alpha^{5/4}\dot{m}^{5/2}m^{3/2}\left(\frac{D_3}{R_0 m}\right)^{-p} \tag{A23}$$

Solving equation A23 for $(D_3/R_0 m)$ gives

$$\left(\frac{D_3}{R_0 m}\right) = \left(\frac{e}{432 m_{\rm e}c}\right)^{1/(1+p)}\left(\frac{R_0}{\pi^3\epsilon^5\kappa_{\rm T}}\right)^{1/2(1+p)}$$

$$* \alpha^{5/4(1+p)}\dot{m}^{5/2(1+p)}m^{1/2(1+p)} \tag{A24}$$

Substituting equation A24 into equation A20, gives

$$W_{\max} = \frac{1}{3^{(4-2p)/(1+p)}} \left(\frac{\pi^{-2+4p} e^4 c^{4p} R_0^2}{2^{2-2p} m_{\rm e}^{2(1-p)} \epsilon^{6-4p} \kappa_{\rm T}^2} \right)^{1/2(1+p)} * z\Gamma\alpha^{(6-4p)/4(1+p)} \dot{m}^{(6-4p)/2(1+p)} m^{1/(1+p)} \quad \text{(A25)}$$

$\dot{m}$ can also be elimanted to give

$$W_{\max} = \frac{1}{6} \left(\frac{3^{2p} e^4 \kappa_{\rm T}^{4-4p}}{4\pi^{8-8p} m_{\rm e} c^{18-16p} R_0^{4-4p} \epsilon^{6-4p}} \right)^{1/2(1+p)} * z\Gamma\alpha^{(6-4p)/4(1+p)} m^{-2(1-p)/(1+p)} L_{rad}^{(6-4p)/2(1+p)} \quad \text{(A26)}$$

The p-dependent formulae in this section can be naturally reduced, if one assumes $p = 1/2$, in the "standard case" for example, as was done in section 2. It may be useful to incorporate such a dependency on the jet spreading (p-index) in assessing maximum proton energy from particularly SS433, due to it's location and rather broad jet, as well as other astrophysical objects.